SPEKTRUM

Mitteilungsblatt der Fachgruppe Spektroskopie
in der Vereinigung der Sternfreunde e.V.
Journal of the Section Spectroscopy of the Society of German Amateur Astronomers

NR. 55 **1 / 2019**

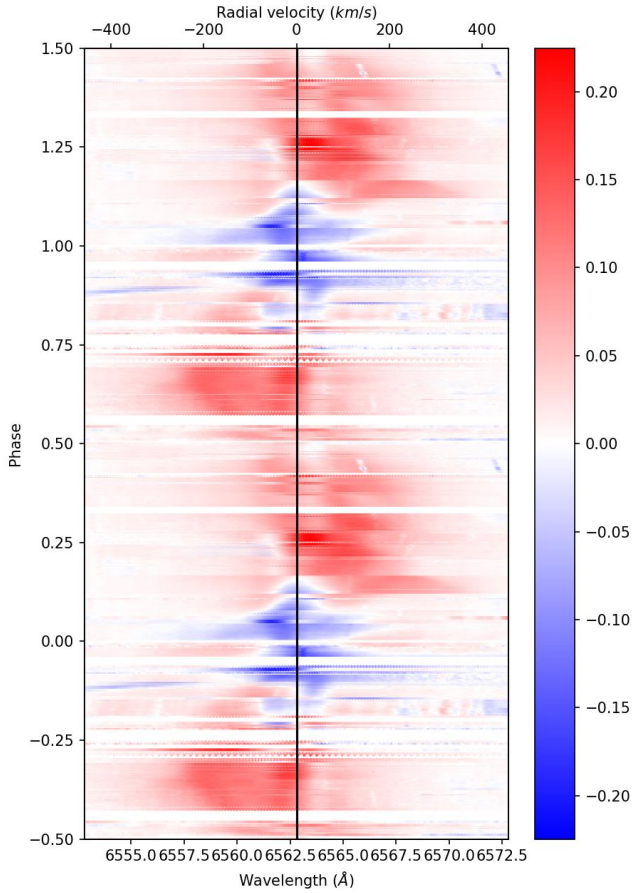

β PERSEI

STARANALYSER UND WINTERSECHSECK OBJEKTIVGITTER

ISSN 2363-5894

Impressum

Spektrum – Mitteilungsblatt der Fachgruppe Spektroskopie in der Vereinigung der Sternfreunde wird herausgegeben von der Fachgruppe Spektroskopie in der Vereinigung der Sternfreunde e.V. Es erscheint halbjährlich als PDF-Ausgabe oder auf Wunsch als Druckversion. Das Journal dient dem überregionalem als auch dem internationalen Erfahrungsaustausch auf dem Gebiet der Astrospektroskopie besonders für Amateure. Dazu können Beiträge in Deutsch oder English publiziert werden. Senden Sie Ihre Beiträge, Auswertungen, Erfahrungen und Kritiken an **Spektrum** zur Veröffentlichung ein, damit andere Spektroskopiefreunde an Ihren Erkenntnissen teilhaben und davon lernen können.

Spektrum – Mitteilungsblatt der Fachgruppe Spektroskopie in der Vereinigung der Sternfreunde is issued twice a year by Fachgruppe Spektroskopie of Vereinigung der Sternfreunde e.V. (spectroscopy section of the German amateur astronomical society). The journal is published as a PDF or as a printed version on special request. The aim of the journal is to be a national and international communication especially for amateurs, on topics related to astronomical spectroscopy. Contributions are welcome in German or English. Please send your papers, results, experiences and reviews to **Spektrum** for publication. The community can then benefit from your experience.

Registriert bei der Deutschen Nationalbibliothek / Registered at Deutsche Nationalbibliothek: DNB 1013413024

ISSN 2363-5894

Die Fachgruppe Spektroskopie im Internet: spektroskopie.fg-vds.de

Die Vereinigung der Sternfreunde e.V. im Internet: www.vds-astro.de

Kontaktadresse (Redaktion, Bestellung gedruckter Ausgaben, Einsendung von Manuskripten)

Dr. Thomas Hunger
Weinbergstraße 12
D-01129 Dresden
thunger03@web.de

Hinweise für Autoren:
Nur durch Ihre Artikel wird Spektrum gefüllt. Die Redaktion behält sich vor, in Rücksprache mit den Autoren Beiträge zu kürzen, anzupassen oder zu ändern. Für die Inhalte der Artikel ist aber allein der Autor verantwortlich. Mit der Einreichung eines Beitrages erklärt der/die Autor(en) die Bereitschaft zur Publikation auch im Journal für Astronomie der VdS e.V.
Reichen sie Ihren Beitrag bitte elektronisch unter Berücksichtigung folgender Regeln ein:
Form des Textes: Senden sie vorzugsweise als unformatierten ASCII-Text. Tabellen mit Tabulatoren getrennt. Ein zusätzliches PDF des formatierten Gesamttextes ist anzuraten.
Aufbau der Artikel: Die Artikel benötigen einen Titel, eine vollständige Adressangabe des Autors / der Autoren, eine Kurzzusammenfassung, den klar gegliederten Artikel mit Einleitung und Zusammenfassung sowie eine vollständige Literaturangabe.
Abbildungen: Bitte getrennt vom Text senden. Empfehlenswert sind hochauflösende JPG, PNG und TIFF.

Hints for authors:
Your article will be edited to fit the style of Spektrum. The editor is responsible for editing the article in close collaboration with the author. The author is in charge of the content in all cases, however. The author(s) give(s) the permission for a further publication of the contribution in the journal of the VdS e.V. (Journal für Astronomie) right with its transfer to the editor of Spektrum. Please send your contribution via electronic mail considering the following rules:
Text: Prepare it as unformatted text (preferably ASCII). Tables: columns separated by tabs. A PDF printout of the whole document is highly recommended.
Article structure: Each article should include a title, an address line of the author(s), an abstract, a clear text body with introduction and conclusion and complete references.
Figures: Please send them separate from text. High resolution JPG, PNG or TIFF files are recommended.

Umschlagfoto: Differenzlinienprofile von β Per aus der Beobachtungsperiode 2014 – 2019. Näheres dazu im Artikel von Bernd Bitnar et al. im Heft.

Inhaltsverzeichnis / Content

Editorial

Liebe Leser des Spektrums,
liebe Fachgruppenmitglieder,

kurz vor Jahresende erhalten Sie die Ausgabe Nr. 55 unserer Zeitschrift. Aus ganz unterschiedlichen Gründen hat sich die Fertigstellung deutlich verlängert, so dass es dieses Jahr auch nur diese eine Ausgabe gibt. Das Warten hat sich aber auf jeden Fall gelohnt.

Die Fachgruppe befindet sich in einer schwierigen Phase. Dies findet unter anderem seinen Ausdruck in einer schon seit Monaten schwachen Nutzung unseres Forums. Von den Vakanzen des Webmasters und des Sprecheramtes ganz abgesehen. Über die (Wieder-)Belebung muss intensiv gesprochen werden! Jeder ist dazu eingeladen.

Dazu bietet sich die im kommenden Juni stattfindende ASpekt 20 an. Ideen aller Art ohne Denkbeschränkung sind höchst willkommen. Bitte denken Sie auch schon jetzt über eigene fachliche Beiträge nach: tragen Sie vor, geben Sie ihre Erfahrungen weiter, stellen Sie ein Poster vor. Nur dadurch kann solch ein Treffen zum Erfolg werden – dies gilt selbstverständlich auch für das geschriebene Wort in Spektrum.

Mit sternfreundlichen Grüßen,
Ihr Thomas Hunger

Dear readers of Spektrum,
Dear members of the section group,

shortly before year's end, you receive issue no. 55 of our magazine. For some different reasons, the completion has been significantly extended. Thus, only this one issue is published. But the waiting time was worth it – in any case.

The section group entered a difficult phase. This finds its expression in an already weak use of our forum for months - quite apart from the vacancies of the webmaster and the speaker. An intensive discussion on the (re-)animation must take place! Everybody is invited.

The section conference ASpekt 20, which will take place next June, will offer a good platform. Ideas of all kinds without thinking restrictions are very welcome. Please also consider an active contribution, give a talk, share your knowledge, present a poster. Only by activities such a meeting can be a success – this of course also applies to the words written in Spektrum.

Clear skies.
Yours Thomas Hunger

Continuum Normalization using Synthetic Spectra

Christian Brock
Sternwarte Gönnsdorf, Weißiger Landstraße 6, 01328 Dresden, Germany, E-mail: christian.brock@posteo.net

Abstract
For a quantitative analysis of measured spectra, an accurate and reproducible continuum normalization is essential. We show how such a normalization can be implemented using the data points of synthetic spectra as reference.

Zusammenfassung
Für die quantitative Analyse gemessenen Spektren ist eine genaue und reproduzierbare Normalisierung des Kontinuums unerlässlich. Wir zeigen, wie eine solche Normalisierung unter Verwendung synthetischer Spektren implementiert werden kann.

Received: 2019-02-10, Revised: 2019-02-18, Accepted: 2019-03-15

1. Introduction

For an amateur project observing the Hα emission of an accretion disc around Algol (β Persei) [1], we needed to compare the observed spectra against synthetic spectra of an B8V star showing no emissions. As the intensity of the emissions is below ten percent of the continuum, we needed a good signal-to-noise ratio (SNR) and a very accurate continuum normalization.

The ESO Midas documentation, Volume B [2], states:
"A frequently used procedure, alternative to the correction for the chromatic response, is to normalize the continuum to unity by dividing the observed spectrum by a smooth approximation of its continuum."

There are several approaches to solve this problem:
- Ref. 3 and 4 use linear approximations of data points at predefined wavelengths, usually one to the left and one to the right of an observed absorption line.
- The software tool Visual Spec [5] allows the user to interactively enter continuum points with the mouse and then uses a "softened" spline to approximate the continuum.
- ESO Midas [2] also allows to enter continuum points interactively, it then uses spline fits by default (see ref. 6, p.502).

All interactive methods have the following drawbacks. They
- depend on expert knowledge of the user,
- are not reproducible,
- require a continuum to be present, which is a problem with cold stars or spectra of a narrow wavelength region around a broad absorption line,
- cannot be used for any but small observation campaigns.

In this paper we argue that all those drawbacks can be overcome using data points from synthetic spectra of the observed stars. For this we need to apply some transformations to the synthetic spectrum.
- For the **wavelength correction** of the synthetic spectrum to fit the observed spectrum we need to consider the radial velocity of the observed star.
- The **spectral resolution** of the synthetic spectrum needs to be changed to match the observed spectrum.

We implemented the normalization using the Python programming language, especially the numpy [7] and astropy [8,9] packages.

2. Methods

2.1 Preparation of the synthetic spectrum

Where to get one
For this work we did not calculate our own spectra. For enthusiasts we recommend having a look at iSpec [10] (see fig. 1). iSpec combines several spectral models under one common interface.

For our work we used the "The POLLUX Database of Stellar Spectra" [11]. It supports more spectral models (see fig. 2) and does not require the installation of additional software.

To choose a spectrum one needs at least the effective temperature, surface gravity, metallicity and rotational velocity of the target star. Such parameters can be found in the Simbad, ref. 12.

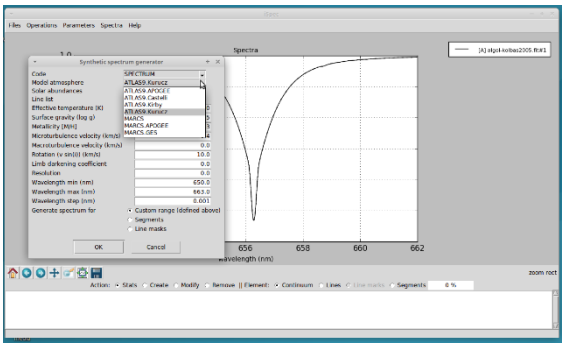

Fig. 1: Screenshot from iSpec [10].

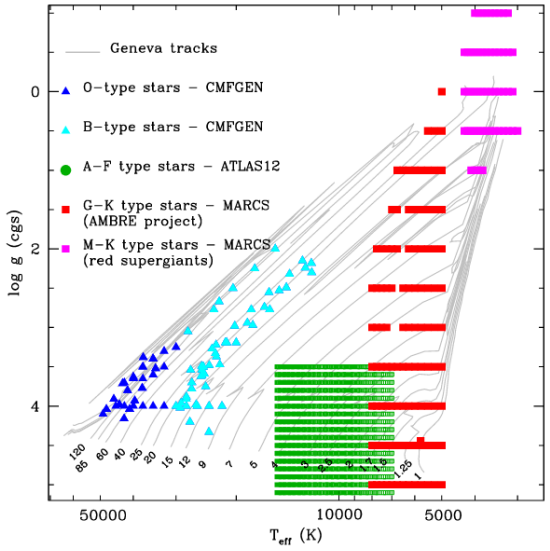

Fig. 2: Spectral models used by "The POLLUX Database of Stellar Spectra", ref. 11.

Applying wavelength correction

For the wavelength correction of the synthetic spectrum to fit the observed spectrum we need to consider the radial velocity of the observed star. For ordinary stars this value can be found in online databases such as Simbad, ref. 12.

For binary or hierarchical star systems one has to model the orbits of all system components [13]. This by itself is a major project and will be subject of a future publication. At the time of this paper we know of no standard software to implement such models.

Here we assume that the radial velocity of the target star in relation to the sun $v_{\star\to\odot}$ is known. We can then calculate the radial velocity of the star in relation to the earthbound observer $v_{\star\to\varphi}$:

$$v_{*\to\earth} = v_{*\to\odot} - v_{\earth\to\odot} \tag{1}$$

$v_{\varphi\to\odot}$ is the heliocentric or barycentric correction - the velocity component toward the target star caused by earth moving around the sun (see fig. 3). It can be calculated using the astropy.coordinates.SkyCoord.radial_velocity_correction method.

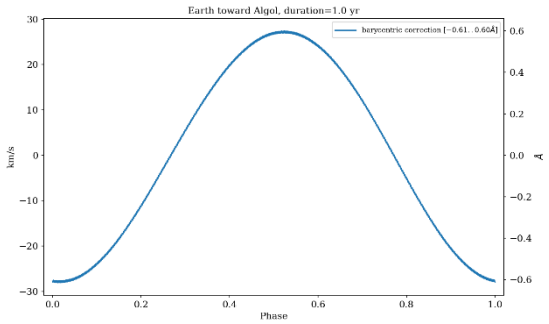

Fig. 3: Barycentric correction for the Algol system during a single year.

Having the stars radial velocity toward earth we can then calculate the wavelength shift by

$$\Delta\lambda_{rv} = \bar{\lambda}\frac{v_{*\to\earth}}{c} \tag{2}$$

with $\bar{\lambda}$ as the center wavelength of the observed spectrum and *c* the speed of light.

It is also possible to derive the redshift from the measured data itself. One can measure the wavelength difference of absorption line minima between the observed and synthetic spectra.

Modifying spectral resolution

We also need to apply the resolution of the observed spectrum *RESOL* to the synthetic spectrum. We do this by convolving the synthetic spectrum with a Gaussian kernel having a standard deviation of

$$\sigma = \frac{\bar{\lambda}}{2.3548\ RESOL} \tag{3}$$

2.3548 is the full width at half maximum of the standard Gaussian. Refer to e.g. ref. 6, p. 320, for an explanation how spectral resolution is defined. The convolution can be performed by the astropy.convolution.convolve method applying a astropy.convolution.Gaussian1DKernel to the spectrum.

2.2 Continuum approximation

For the continuum approximation, the "smooth approximation" as explained above, we assume that our continuum can be modeled by a polynomial p_n of a given degree n with additional Gaussian noise.

$$cont = p_n + \epsilon \tag{4}$$

Masking

Before we continue one additional thought: We may want to exclude some wavelength regions of the observed spectrum when we know in advance that the observed spectrum does differ significantly from the synthetic one. In our Algol example we wanted to measure emission features in the center of the Hα line. This exclusion can be done by masking that regions. Additionally, excluding high slope regions makes the approximation more robust against redshift and resolution errors.

Getting the polynomial

Having all in place we are able to calculate a smoothed approximation of the continuum:

$$cont_{approx} = \arg\min_{p_n} \sum_{\lambda} \left(p_n - \frac{observed}{synth} \right)^2 \tag{5}$$

We sum over the wavelengths of the unmasked data points. Fitting can be done with the `numpy.polyfit` method.

What degree?

The polynomial degree depends on the fitted wavelength range and on properties of the spectrograph. This is demonstrated in fig. 4.

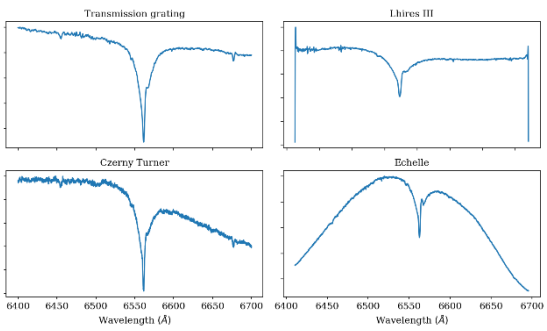

Fig. 4: Hα measured by four different spectrographs. One can see how polynomials of different degree may be required to fit the different spectra. The Echelle requires a degree of n = 5 while the others only need n = 3.

In general, as the number of data points vastly exceeds the polynomial degree, the approximation is very robust against oversampling. In the Algol project we usually use n = 5. If unsure one can use the AIC[1] [14] to choose the degree that fits the data best.

About Signal-to-noise ratio

Equation 5 minimizes the noise term ε in equation 4. We see that our continuum approximation minimizes that noise, i.e. maximizes the signal-to-noise ratio (SNR). The `argmin` argument is called residual. It can be used to calculate the SNR

$$residual = \sum_{N} \left(p_n - \frac{observed}{synth} \right)^2 \tag{6}$$

$$\sigma_\epsilon = \sqrt{\frac{residual}{\|N\|}} \tag{7}$$

$$SNR = 1/\sigma_\epsilon \tag{8}$$

N are the data points used for the approximation, the measured points of the observed spectrum (not removed by masking). The residual is one of the results of `numpy.polyfit`. ||N|| is the number of data points used for the approximation[2].

2.2 Normalization

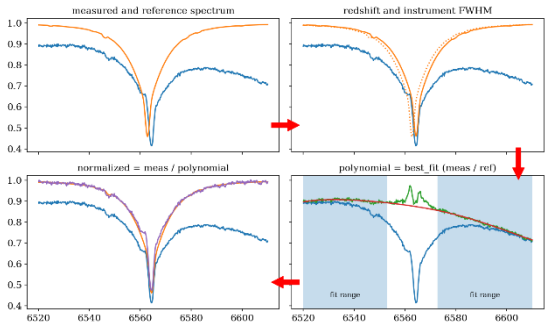

Fig. 5: The entire normalization process containing, wavelength calibration, convolution with the instrument resolution, calculation of the best fitting polynomial and finally the normalization. The fit, the red curve in the lower right plot, is calculated in the blue area -- the line center, the white area, is masked.

Now, the normalized spectrum is

$$spec_{norm} = \frac{observed}{cont_{approx}} \tag{9}$$

[1] Akaike information criterion

[2] The 1 in the nominator of equation 8 is actually misleading. It should be replaced by the maximum or the average of the observed spectrum.

Fig. 5 finally shows the entire data reduction process.

4. Conclusion

We have shown that data points of synthetic spectra can be used for continuum normalization. The approach is very accurate, reproducible, robust against parameter variations and can be used in an automatic pipeline of observation campaigns. It is preferable to manual procedures implemented in many tools. We further displayed that the least square fit of the continuum approximation optimizes SNR.

Software

The author implemented the entire normalization as Python command line tool. It can be downloaded under
https://pypi.org/project/algol-reduction/.

Acknowledgments

The author would like to acknowledge the help received from the spectroscopic community, especially his local Dresden group and the people running the Dresden Gönnsdorf Observatory. Special thanks go to Bernd Bitnar, Enrico Gerlach, Thomas Hunger, Josefine Liebisch and Ulrich Waldschläger (in alphabetical order)

References

[1] B. Bitnar and U. Waldschläger, SPEKTRUM - Mitteilungsblatt der Fachgruppe Spektroskopie in der Vereinigung der Sternfreunde e.V. 52 (2017) 4
[2] ESO (1999). ESO-MIDAS documentation. https://www.eso.org/sci/software/esomidas/doc/index.html. Accessed on 2019-02-05
[3] M.T. Richards, Astrophys. J. Supp, 86 (1993) 255
[4] J. Liebisch, SPEKTRUM - Mitteilungsblatt der Fachgruppe Spektroskopie in der Vereinigung der Sternfreunde e.V., 54 (2018) 17
[5] V. Desnoux, Visual Spec tutorial. http://www.astrosurf.com/vdesnoux/tutorial.html. Accessed on 2019-02-05
[6] D. Sablowski, D. and L. Schanne, Astrophysikalische Instrumentierung und Messtechnik für die Spektroskopie., Eigenverlag, 2018
[7] T. Oliphant, NumPy: A guide to NumPy. Trelgol Publishing. (2006-) Accessed on 2019-02-08
[8] Astropy Collaboration: T.P. Robitaille, et al., A&A 588 (2013) A33
[9] A.M. Price-Whelan et al., Astro. J. 156 (2018) 123
[10] S. Blanco-Cuaresma et al., A&A 569 (2014) A111.
[11] A. Palacios et al., A&A 516 (2010) A13
[12] M. Wenger et al., Astrophysics and Space Science, 143 (2000) 9
[13] E. Gerlach, 2015, unpublished
[14] H. Akaike, IEEE Trans. Automatic Control AC-19, (1974) 716

During daytime **Christian Brock** programs algorithms to optimize cellular networks. At night he attends to visitors at the Dresden-Gönnsdorf Observatory, supervises students, does some visual observations by himself and cooperates in the Dresden spectroscopy group.

Das Wintersechseck mit dem StarAnalyzer 100

Oskar Pircher
Flurweg 13, 83119 Obing, Germany, E-Mail: pircher@fpircher.de

Zusammenfassung
Dieser Artikel beschreibt die Ergebnisse einer spektroskopischen Beobachtung der Sterne des sogenannten „Wintersechseckes“ sowie von Castor und Beteigeuze mit dem StarAnalyzer 100. Ein Vergleich zwischen Castor A, Castor B und Sirius führt zu einer Erörterung, ob Elemente, die in Am-Sternen überhäufig vorkommen, nachgewiesen werden können – ohne positives Ergebnis. Zuletzt wird gezeigt, dass die Signatur von Natrium bei 5890 und 5896 Å zwar schwach, aber vorhanden ist.

Abstract
This article is a report of a spectroscopic observation of the “winter circle“ with the StarAnalyser 100. Castor and Betelgeuse are included as well. A comparison between Castor A, Castor B and Sirius leads to a discourse, whether some elements, that should be in abundance in Am stars, could be detected – without evidence so far. At least it is shown, that the signature of sodium at 5890 and 5896 Å is weak but present in the profiles of the before mentioned stars.

Received: 2019-05-29, Revised: 2019-08-01, Accepted: 2019-10-04

1. Einführung und Verfahrenbeschreibung

Das Wintersechseck besteht aus den Sternen Capella im Sternbild Fuhrmann, Aldebaran im Sternbild Stier, Rigel im Sternbild Orion, Sirius im Sternbild Großer Hund, Prokyon im Sternbild Kleiner Hund und Pollux im Sternbild Zwillinge. Diese am Winterhimmel sichtbaren Sterne bilden die Ecken eines unregelmäßigen Sechseckes. Es ist kein Sternbild nach der Bezeichnung der Internationalen Nomenklatur.

Die scheinbaren visuellen Helligkeiten der Sterne des Wintersechsecks sind größer als 1. Größenklasse (< 1 mag). Sie sind daher lohnende Ziele für eine Untersuchung für den StarAnalyzer 100 in Verbindung mit einer Planetenkamera. Die im Folgenden vorgestellten Ergebnisse beruhen auf Aufnahmen vom 31.03.2019, gewonnen mit der Planetenkamera Celestron SkyRis132 M mit vorgesetztem StarAnalyzer 100 im Fokus eines Newton-Reflektors R 135 S von Vixen (135 mm Öffnung, 720 mm Brennweite). Von jedem Stern, zusätzlich auch noch von Beteigeuze und Castor, habe ich 10 Aufnahmeserien zu je 10 Bildern aufgenommen. Zwischen jeder Aufnahme wurde das Teleskop sowohl in Rektaszension und Deklination um einige Pixel versetzt. Mit diesem Dithering sollen das Rauschen und Fehler einzelner Pixel ausgemittelt werden. Auf den Abzug von Dunkelbildern und von Flatfieldaufnahmen habe ich verzichtet. Mit Ausnahme von Sirius und Castor habe ich jeweils die Bilder aus 4 Serien zu einem Summenbild addiert, aus denen ich das jeweilige Spektrum ausgeschnitten habe. Aus diesen Ausschnitten wurden mit der Software Visual Spec (Vspec) die Spektralprofile erzeugt und kalibriert [1]. Bei Sirius und Castor habe ich jeweils ca. 20 Bilder aus unterschiedlichen Serien mit ausgesucht geringer Punktspreizung addiert. Die Dispersion der Spektren beträgt 7,91 Å/Pixel. Näheres zum Verfahren findet sich in Referenz 2. Daten zu den einzelnen Sternen und den jeweiligen Aufnahmeeinstellungen finden sich im Anhang.

2. Sternspektren

Rigel

Der späte B-Überriese Rigel (β Orionis) zeigt in dem für das eingesetzte Setup zugänglichen Spektralbereich wenig Absorptionslinien, siehe Abb. 1. Von den Linien der Balmer-Serie sind gerade noch Hβ, Hγ und Hδ zu erkennen und bei der Linie des einfach ionisierten Magnesiums mag eine noch schwache Linie des atomaren Heliums einen Beitrag leisten. Ansonsten sind die Helium-Linien zu schwach, um erkennbar zu sein. Da sowohl die Effizienz des auf 500 nm geblazten StarAnalyzers als auch die Empfindlichkeit des Sensors der Kamera zu kürzeren Wellenlängen hin rasch abfallen, B-Sterne das Maximum ihrer Strahlungsintensität jedoch im UV besitzen, sind diese Sterne wenig für die Untersuchung mit dem verwendeten Equipment geeignet. Zudem zeigen Überriesen aufgrund der ausgedehnten Atmosphäre nur schmale Linien.

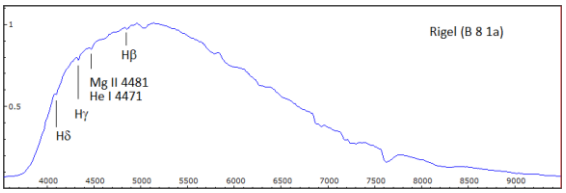

Abb. 1: Spektrum von Rigel (α Ori) als Screenshot aus VSpec.

Capella

Capella ist ein Doppelstern, bestehend aus zwei Komponenten der Spektralklassen G1 und K0, beide der Leuchtkraftklasse III (Riesen) zugehörig. Ein wegen des als G3-gesamtklassifizierten Summenspektrums naheliegender Vergleich mit dem in Anlage R des in Band 1 des Bonner Spektralatlas [3] veröffentlichten Spektrum der Sonne führte zu der in Abb. 2 gezeigtem Spektralprofil eingetragenen Zuordnungen von Elementen zu den Absorptionslinien, die sich wegen der geringen Auflösung und Dispersion vielfach als Überlagerung („Blends“) zeigen. Immerhin deutet sich die Unterscheidbarkeit von CrI bei 4646 Å und FeI bei 4668 Å an. Daraus lässt sich eine Auflösung von R ≈ 200 ableiten, was gut zum allgemein berichteten Auflösungsvermögen passt.

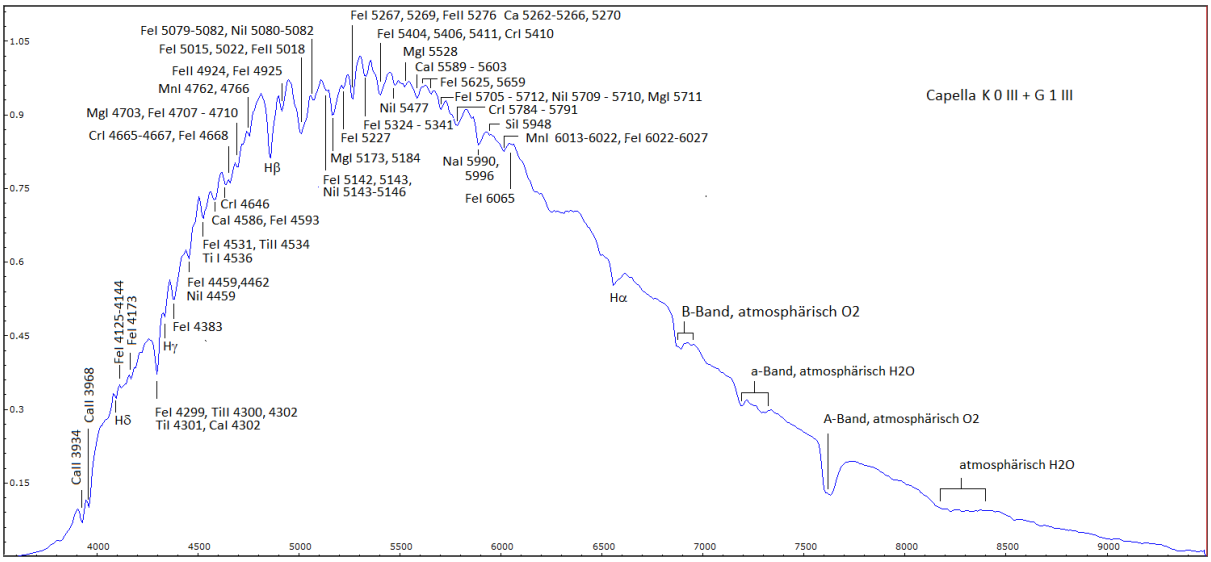

Abb. 2: Spektrum von Capella (α Aur) als Screenshot aus VSpec. Absorptionslinien nach einem Vergleich mit dem Sonnenspektrum sind benannt.

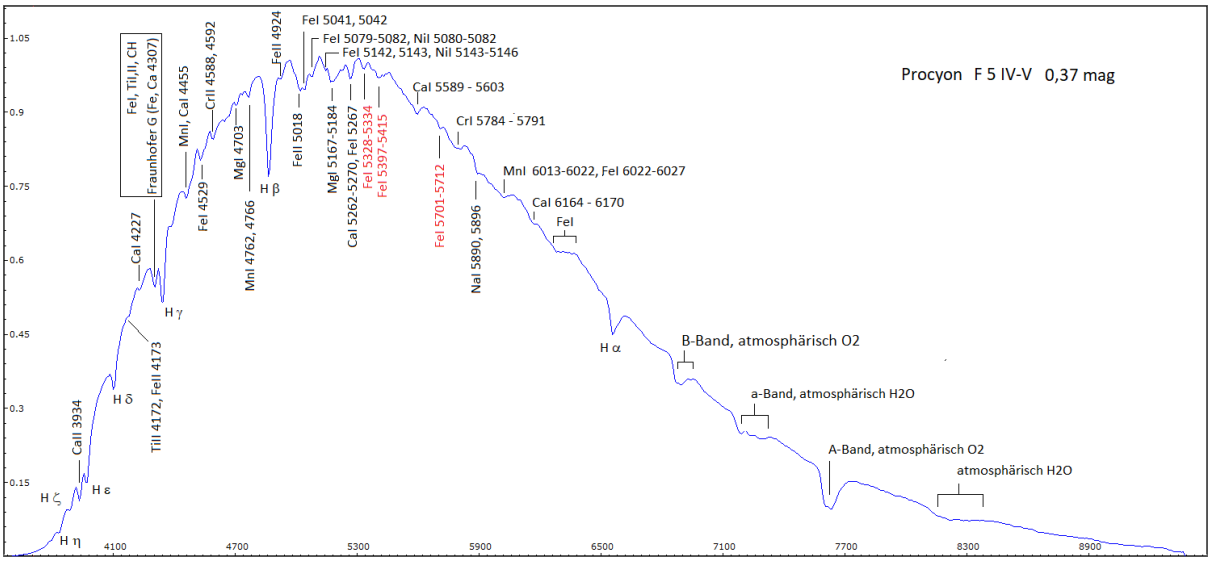

Abb. 3: Spektrum von Procyon (α CMi) als Screenshot aus VSpec.

Procyon

Weniger zahlreich und ausgeprägt zeigen sich mit Ausnahme der Linien der Balmerserie des Wasserstoffes die Absorptionslinien beim F5 „Fast-Unterriesen“ Procyon (Abb. 3). Grundlage für die Zuordnung der Elemente war wieder Band I des Bonner Spektralatlasses.

Pollux

Die Spektral- und Leuchtkraftklasse von Pollux ist gleich der Komponente A von Capella (K0III). Statt einer erneuten Wiedergabe der Elemente-Zuordnung sei an dieser Stelle ein Vergleich mit den Spektralprofilen von Prokyon und Capella gezeigt, Abb. 4. Die Profile sind auf den Bereich zwischen 5300 und 5400 Å normiert.

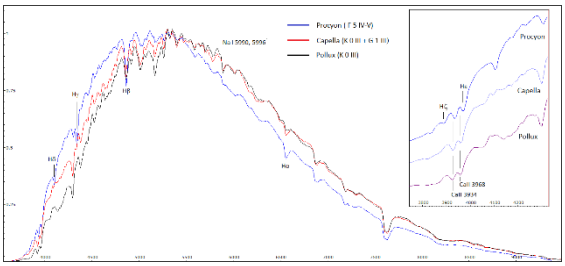

Abb. 4: Spektrum von Pollux (β Gem) im Vergleich zu Capella und Prokyon als Screenshot aus VSpec. Insert: Blauseitiger Vergleich der Spektren.

Erkennbar sind der bei kürzeren Wellenlängen beginnende „frühere“ Anstieg als auch der frühere rotseitige Abstieg der Intensität bei Procyon. Auch bei Capella ist gegenüber Pollux ein früherer Anstieg der Intensität bemerkbar (erklärbar mit der Komponente G1-Komponente), während sich beim Abstieg der Intensität die K0-Komponente in einem nahezu identischen Verlauf mit den Werten für Pollux bemerkbar macht.

Deutlich zu erkennen ist die zunehmende Schwächung der Hα-Linie zur späteren Spektralklasse hin, dafür eine zunehmende Intensität der Natrium-Doppellinie bei 5890 und 5896 Å. Zur besseren Übersichtlichkeit sind die Kalzium-Linien CaII H und K bei Capella und Pollux gegenüber der Hε- und der Hζ-Linie im Insert dargestellt.

Aldebaran und Beteigeuze

Deutlich anders als das Spektralprofil des K0-Sterns Pollux zeigt sich das Profil des K5-Sterns Aldebaran in Abb. 5, dass schon mehr Ähnlichkeit mit dem frühen M-Überriesen Beteigeuze aufweist. Die markantesten Absorptionslinien bestehen aus Blends von Molekülbanden des Titanoxids. Der Vergleich im Insert zwischen Aldebaran und Capella, zeigt, dass auch die atmosphärischen Bänder a und A zusätzlich von TiO-Banden überlagert werden. Noch intensiver werden die TiO-Absorptionen bei Beteigeuze, hier sind die differenzierten Signaturen des a-Bandes bereits nicht mehr zu erkennen.

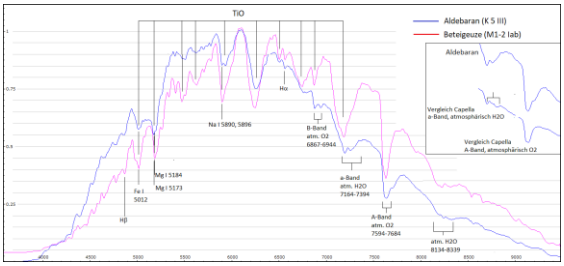

Abb. 5: Spektren von Aldebaran (α Tau) und Beteigeuze (α Ori) als Screenshot aus VSpec. Insert: Vergleich des rotseitigen Spektrums von Aldebaran mit Capella.

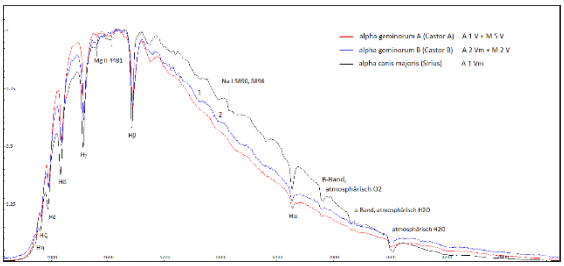

Abb. 6: Spektren von Castor A&B (α Gem) und Sirius (α CMa) als Screenshot aus VSpec..

Castor und Sirius

Nicht zum Wintersechseck zählt α Geminorum (Castor), ein Mehrfachsystem mit den Hauptkomponenten A und B, das an dieser Stelle wegen der ähnlichen Spektralklasse zusammen mit der noch ausstehenden „Ecke“ des Wintersechseckes in Gestalt von Sirius dargestellt werden soll (Abb. 6). Die Hauptkomponenten Castor A und B zeigten sich im Teleskop so weit getrennt, dass die Spektren beider Sterne gerade noch getrennt aufgenommen werden konnten. Castor A ist ein A1V-Stern mit einem Begleiter mit vermuteter Spektralklasse M5V. Die Spektralklasse von Castor B ist A2Vm einem M2V Begleiter. Die Signaturen der beiden M-Begleiter sind in den Spektralprofilen wegen der erheblich geringeren Leuchtkraft nicht zu bemerken.

Alle Profile sind auf den Bereich von 4900 Å normiert. Es fällt auf, dass das Profil von Sirius scheinbar zu längeren Wellenlängen hin verschoben ist. Hier macht sich die unterschiedliche Absorption und Streuung der blauen Lichtanteile durch die Erdatmosphäre bemerkbar. Sirius stand zum Aufnahmezeitpunkt nur ca.

16° über dem Horizont, Castor 64°. Auch die atmosphärischen Linien sind aufgrund der niedrigen Höhe bei Sirius deutlich intensiver als bei den Komponenten von Kastor.

Erkennbar unterscheiden sich die Profile von Castor B und Sirius im Bereich von 5100 bis 6100 Å deutlich vom Profil von Castor A. Die Versuchung liegt nahe, diese Erscheinung damit in Verbindung zu bringen, dass Castor B und Sirius Am-Sterne sind. Gemäß Ref. 4 weisen Am-Sterne Überhäufigkeiten u.a. der Elemente Kupfer (Cu) und Yttrium (Y) sowie der Seltenen Erden auf. In den Teilspektren in Abb. 7 wurden die Spektralprofile zwischen 4400 und 6400 Å mittels einer Ausgleichkurve (Splines) normiert. Dadurch werden Linien, wie z.B. Mg II bei 4481 Å, besonders stark hervorgehoben. Ein Artefakt dieser Bearbeitung ist die scheinbare Emission und zentrale Absorption der Hβ-Linie, was so im Original nicht sichtbar ist.

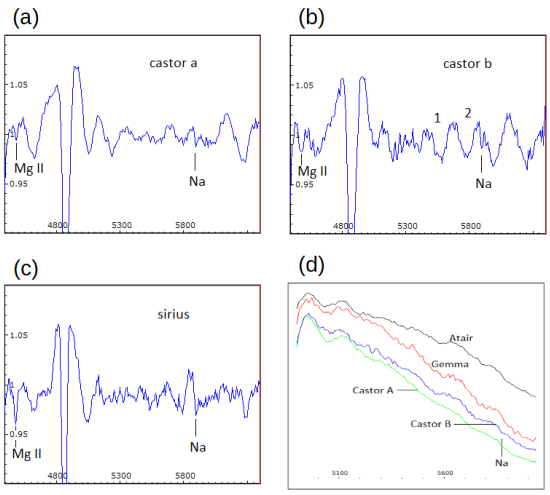

Abb. 7: Normierte Teilspektren von (a) Kastor A, (b) Kastor B und (c) Sirius. (d) Vergleich der nichtnormierten Spektren von Kastor A & B mit den vergleichbaren Sternen Gemma und Atair zum gezielten Nachweis von Metallen.

Eine gezielte Suche nach Cu, Y und Europium (Eu) als einem dem häufigen Vertreter der Seltenen Erden im Spektralprofil von Castor B in den mit 1 und 2 markierten Bereichen mittels der Funktion „Elements“ in Vspec ergibt eine Vielzahl von zu erwartenden Spektrallinien dieser Elemente in den genannten Bereichen. Jedoch zeigt ein Vergleich im Abb. 7d mit den Spektralprofilen von Gemma (α Coronae Borealis) und Atair (α Aquliae), dass diese nicht als Am Sterne klassifizierten Sterne ebenfalls mit Castor B vergleichbare Strukturen aufweisen. Damit kann ein Zusammenhang der Bereiche 1 und 2 mit den Elementhäufigkeiten von Am-Sternen hier nicht hergestellt werden. Für die bei Castor B auffallenden Linien um 5300 Å bei konnte ich keine Übereinstimmung mit den vorgenannten Elementen finden.

3. Untersuchung zur Evidenz von Linien

In allen drei Profilen Abb. 7a-c findet sich bei ca. 5990 Å eine schwache Absorptionslinie, bei der es sich um die Doppellinie des neutralen Natriums bei 5990 und 5996 Å (Fraunhofersche D-Linie, im Folgenden Na D genannt) handeln könnte. Die beiden Linien können mit dem verwendeten Setup nicht aufgelöst werden.

Zur Abschätzung, ob sich die Na D-Linie vom Rauschen unterscheiden lässt, wird wie folgt vorgegangen:

- Aus dem Summenbild der überlagerten Einzelaufnahmen von Castor B wurde aus dem Spektrum ein Streifen von 750 Pixeln Breite und 3 Pixeln Höhe ausgeschnitten. Dieser Streifen wurde auf 1 Pixel Höhe zu einem 1D-Spektrum aufaddiert („gebinnt“).
- Gleichermaßen wurde aus einem Bereich des Summenbildes über dem Spektrum ein Streifen von 750 x 3 Pixel ausgeschnitten, daraus wurde ebenfalls ein 1 D-Spektrum des Rauschens erstellt.
- Die absoluten Intensitätswerte pro Pixel ADU (Analog-Digital-Units) dieser 1 D-Spektren wurden in ein Tabellenkalkulationsblatt ausgelesen.

Betrachtet wurden im Folgenden:

- Die ADU im Bereich von 7 Pixeln um die vermutete Na D-Linie im Spektrum von Castor B.
- Die ADU im Bereich bei von ebenfalls 7 Pixeln der numerisch größten Varianz im Spektrum des Rauschens.

Da das Kontinuum im Bereich der vermuteten Na D-Linie in diesem Bereich weitgehend linear um 18 ADU/Pixel fällt, wurde zur besseren Vergleichbarkeit mit dem Rausch-Spektrum den jeweils folgenden Pixeln ein entsprechender Wert wie folgt hinzuaddiert:

$$ADU_{neu} = ADU_{n=1} + 18(n\text{-}1) \qquad (1)$$

wobei n die laufende Nummer des Pixels und $ADU_{n=1}$ der Wert des ersten Pixels bedeuten.

In Abb. 8 wurden die Intensitätsverläufe im Bereich der vermuteten Na D-Linie (Spektrum Castor B) und des Bereichs der größten Varianz des Rauschens gegenübergestellt.

Während im Spektrum von Castor B ein sich über mehrere Pixel erstreckender, einer Absorptionslinie entsprechender Verlauf zu erken-

nen ist, bildet das Profil des Rauschens bei Pixel Nr. 2 einen deutlichen Peak, während der weitere Verlauf sich im Rahmen der Standard-Abweichung von ca. 6 ADU bewegt. Diese Signatur des Rauschens wäre also, sollte sie sich zufällig in ähnlicher Weise im Spektrum von Castor B an der Stelle der Natrium D-Linie wiederholen, nicht geeignet, die Signatur einer Absorptionslinie vorzutäuschen. Verbunden mit der Tatsache, dass sich auch bei den Spektren von Castor A und Sirius exakt an gleicher Stelle diese Linie abzeichnet, spricht dafür, dass es sich hierbei wirklich um die Signatur der Na D-Linie handelt.

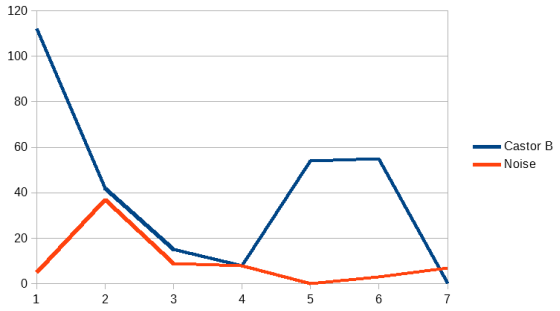

Abb. 8: Vergleich des linearisierten Spektrums von Castor B im Bereich der vermuteten Na D-Linie zu einem Vergleichsspektrum ohne Sternsignal („Noise“).

4. Fazit

Die vorgenommenen Beobachtungen, nachfolgenden Auswertungen sowie Überlegungen haben es mir erlaubt, die Möglichkeiten und Grenzen des StarAnalysers 100 besser kennenzulernen. Messungen der Halbwertsbreite (FWMH) ergeben in der Regel ein Auflösungsvermögen von ca. 250. Es liegt damit zwar deutlich über den Angaben der Herstellers Paton Hawksley, ermöglicht jedoch nur in eingeschränkter Weise die eindeutige Zuordnung von Elementen zu Absorptionslinien, sieht man von den Linien Balmerserie des Wasserstoffes ab. Meist sind die erkennbaren Linien um Blends mehrerer Linien verschiedener Elemente. Jedoch zeigen Profile von Sternen unterschiedlicher Spektralklasse erkennbare Unterschiede hinsichtlich des Intensitätsverlaufs im Kontinuum. Auch kann die Veränderung der Absorptionslinien von den frühen zu den späten Sternen verfolgt werden. In diesen Vergleichen besteht der Reiz von Beobachtungen mit dem StarAnalyser.

Literatur

[1] Desnoux, Valerie: VSpec, http://astrosurf.com/vdesnoux/
[2] Pircher, Oskar: http://spektroskopie.vdsastro.de/files/pdfs/StarAnalyzer_Pircher.pdf
[3] Seitter, Waltraut Carola: Atlas für Objektiv Prismen Spektren, Bonner Spektralatlas I, Ferdinand Dümmlers Verlag, Bonn, 1970
[4] Kahler, James B.: Sterne und ihre Spektren, Spektrum Akademischer Verlag GmbH, Heidelberg, Berlin, Oxford, 1994
[5] Wikipedia:
Aldebaran: https://en.wikipedia.org/wiki/Aldebaran
Beteigeuze: https://en.wikipedia.org/wiki/Betelgeuse
Capella: https://en.wikipedia.org/wiki/Capella
Castor: https://en.wikipedia.org/wiki/Castor_(star) & https://de.wikipedia.org/wiki/Castor_(Stern)
Pollux: https://en.wikipedia.org/wiki/Pollux_(star)
Procyon: https://en.wikipedia.org/wiki/Procyon
Rigel: https://en.wikipedia.org/wiki/Rigel & https://de.wikipedia.org/wiki/Rigel
Sirius: https://en.wikipedia.org/wiki/Sirius

Als Geschäftsleitender Beamter einer kleinen Gemeinde beruflich zwar eher fachfremd - jedoch seit früher Jugend von der Astronomie begeistert - widmet sich **Oskar Pircher** seit gut zwei Jahren der Spektroskopie. Als Mitglied von Astronomie im Chiemgau e. V. hatte er erhebliche Anteile an der Gründung der Solarstromsternwarte im Wildpark Oberreith und gestaltet dort öffentliche Beobachtungsabende. Weiterhin betreibt er noch hochauflösende Mond- und Planetenfotografie.

Anhang

Bayer	Name	Aufnahmedatum	Aufnahmezeit (UT)	Belichtungszeit [µs]	Kamera-Gain
α Tauri	Aldebaran	31.03.2019	19:12:36	250	74
α Orionis	Beteigeuze	31.03.2019	19:21:42	250	32
α Aurigae	Capella	31.03.2019	19:39:59	166,5	32
α Geminorum	Castor A Castor B	31.03.2019	19:33:59	250	109
β Geminorum	Pollux	31.03.2019	19:29:05	250	83
α Canis Minoris	Procyon A	31.03.2019	19:24:41	250	38
β Orionis	Rigel A	31.03.2019	19:07:16	250	83
α Canis Majoris	Sirius A	31.03.2019	18:51:45	68,7	32

Tab. 1: Aufnahmedaten der Objekte. Aufnahmezeit ist der Beginn der ersten Serie. Der Kamera-Gain (Signalverstärkung) kann im Bereich 32-2.000 für die verwendete Kamera eingestellt werden.

Bayer	Spektrum	Scheinbare Helligkeit [mag]	Masse [$M_\odot$]	Radius [$R_\odot$]	Leuchtkraft [$L_\odot$]	Effektiv-temperatur [K]	Fe/H
α Tau	K5III	0,87 var	1,5±0,3	44,2±0,9	439±17	3900±50	-0,15±0,2
α Ori	M1-2Ia-Iab	0,5 var	$11,6^{+5}_{-3,9}$	950-1200	90.000-120.000	3590	0,05
α Aur	G3III = K0III + G1III	0,08 var	2,57 / 2,48	11,98±0,57 / 8,83±0,33	78,7±4,2 / 72,7±3,6	4970±50 / 5730±60	-0,04±0,05
α Gem A	A1V + dM1e (A1VM + M5V)	1,93	2,76[1] (2,15 / 0,5)	2,4 (2,3 / 0,79)	(37,8 / 0,88)	10286	0,98
B	Am + dM1e (A2Vm + M2V)	2,97	2,98[2] (1,7 / 0,5)	3,3 (1,6 / 0,72)	(14 / 0,88)	8842	-280%
β Gem	K0III	1,14	1,91±0,09	8,8±0,1	43	4666	-0,07±0,19
α CMi	F5IV[3]	0,034	1,499±0,031	2,048±0,025	6,93	6530±50	-0,05±0,03
β Ori	B8Ia	0,13 var	21±3	78,9±7,4	120.000[4] (40.600)	12100±150	0,06±0,1
α CMa	A0m A1Va	-1,47	2,063±0,023	1,711	25,4	9940	0,5

Tab. 2: Objektdaten nach Ref. 5. Die Werte sind dem englischsprachigen Wikipedia entnommen. Die in Klammern angegebenen Werten entstammen dem deutschsprachigen Wikipedia, sofern deutlich vom englischen abweichend.

[1] Die Angaben im englischsprachigen Wikipedia sind nicht nachvollziehbar. Der massereichere Stern wäre der leuchtkraftschwächere!

[2] Die Angaben im englischsprachigen Wikipedia sind nicht nachvollziehbar. Der massereichere Stern wäre der leuchtkraftschwächere!

[3] Der Begleiter ist ein Weißer Zwerg mit m_{vis} = 10,7 mag und trägt vermutlich nicht zum Spektrum bei.

[4] bolometrisch

Objective Gratings for Amateurs

Uwe Zurmühl
Sandstraße 8a, 31180 Giesen, Germany, E-Mail: uwe.zurmuehl@t-online.de

Abstract
This article is the follow-up of a paper about transmission gratings used in the convergent beam published in "Spektrum" No. 51 from 2016 [1]. In this article the application of transmission gratings in the parallel beam in front of a telescope optics is discussed. Resolutions of more than R = 20,000 now become feasible using a grating with 1200 L/mm. A further advantage is the nearly linear relation between beam deviation and wavelength, thus easing spectrum calibration. Besides this, the whole construction is the simplest way to build a spectrograph, in other words a true "minimalist approach".
Currently, a variety of affordable blazed transmission gratings is available for the amateur. With a range in size up to 5x5 cm², spectroscopy of stars up to about 6 mag is possible. Because there are practically no additional costs for this simple spectrograph itself, an easy and affordable way to a "low cost and high-resolution spectroscopy" for amateurs is offered. The paper discusses the opportunities and restrictions of objective gratings based on experiences gained with various setups.

Zusammenfassung
Dies ist eine Fortsetzung des Artikels im Spektrum Nr. 51 von 2016 [1], in welcher jetzt anstelle des Einsatzes von Transmissionsgittern im konvergenten Strahl die Benutzung von Objektivgittern beleuchtet wird. Durch das Anbringen eines Gitters im parallelen Strahlengang vor der abbildenden Optik wird nun auch der Bereich hoher Auflösung zugänglich, beim Einsatz eines 1200 L/mm-Gitters etwa mit R > 20.000. Ein weiterer Vorteil besteht im in guter Näherung linearem Zusammenhang zwischen Ablenkung und Wellenlänge, was die Kalibrierung der Spektren deutlich erleichtert. Dabei stellt der gesamte Aufbau prinzipiell den am einfachsten zu realisierenden Spektrographen dar und somit einen echten "minimalistischen Ansatz".
Derzeit stehen dem Amateur kostengünstige Blazegitter zur Verfügung, die mit einer Größe bis zu 5x5 cm² die Spektroskopie von Sternen mit einer Helligkeit bis herunter zu ungefähr 6 mag erlauben. Da ansonsten praktisch keine weiteren Kosten für den eigentlichen Spektrographen anfallen, wird hiermit der Weg zu einer sehr preisgünstigen, hochauflösenden Spektroskopie eröffnet. Die grundsätzlichen Möglichkeiten und Einschränkungen für den praktischen Einsatz von Gittern werden im Folgenden anhand eigener Erfahrungen diskutiert.

Received: 2019-03-12, Revised: 2019-08-03, Accepted: 2019-10-11

1. Introduction

Historically, prisms were the initial dispersion elements to be applied for spectroscopic research in astronomy - first visually, later aided by photographic means. In the beginning slit-less configurations of prisms in front of the telescope's objective were used, allowing the study of point-like light sources. Later, the slit-based spectrographs came up enabling the spectroscopy of extended objects.

200 years ago, Joseph von Fraunhofer was the first producing gratings suitable for spectroscopy. In the last years of his life he was able to build glass-based gratings with more than 400 L/mm (lines/mm) and to perform spectroscopic experiments with them [2]. However, it took over a century before gratings could compete with prisms in terms of efficiency. Nowadays, the main components of most modern spectrographs consist of (reflection-)gratings. Furthermore, the vast majority of setups use the light collected in the focal plane of today's large aperture telescopes. Important exceptions were the star spectroscopy survey projects usually performed with objective prisms. The main goal was spectral classification. One famous example is the comprehensive "Bonner Spectral Atlas" by W.C. Seitter [3,4]. Normally, glass prisms were used for such purposes, whereas objective gratings are rare exceptions. In 1918, M. Wolf applied a grating made of 318 wires with a diameter of 730 mm in front of a 71 cm reflector. With this very low-resolution setup he tried to perform coarse spectral classification [5]. In 1998, M. Köbberling published a self-made amateur's version with a similar layout. He used an objective grating built from fishing line in front of a Celestron 8 telescope [6]. Until this time, the attempts for objective grating usage where hampered for amateurs by the lack

of suitable grating pieces and the low sensitivity of photographic emulsions.
With the advent of affordable CCD sensors and blazed transmission gratings the situation has changed completely. For today's amateurs, particularly at the beginner level, small sized transmission gratings are very popular, especially the "Star Analysers" from Paton Hawksley Inc. [7]. Those are available with 100 L/mm (SA100) and 200 L/mm (SA200) and come in a standard 1,25" mount. When used in a convergent beam configuration, these gratings allow to record low to medium resolution spectra in a very comfortable way [1,8-10].

For the special case of using such gratings in front of the aperture (objective grating spectrographs), there seems to be a significant lack for both experimental and theoretical papers. When searching for examples of objective transmission gratings in the amateur scene, one mainly finds results for the Star Analysers [8-10]. Most of the described applications use these gratings in front of telephoto lenses. By doing so, the effective aperture is reduced to the grating's size of approx. 1" diameter. Therefore, spectra with a reasonable S/N ratio can only be obtained for rather bright objects or very long exposures. Nevertheless, as shown below, such small-size gratings may be fine for first experiments and gaining experience with this technique.

For more serious work, however, larger gratings are needed. The gratings with the largest area which are still affordable (price in the 200 €-range) offer an effective area of 5x5 cm². In this paper, experiences gathered with gratings from Thorlabs [11] will be described. The currently used versions are the 300 L/mm, 600 L/mm, 830 L/mm and 1200 L/mm transmission gratings all ruled for the visual wavelength range. As will be shown below, the potential resolution increases with the grating's dispersion proportional to the L/mm number. At the same time, the sensitivity and recordable wavelength range decreases. To get the optimum performance for a specific project, the appropriate grating has to be chosen accordingly.

Only few examples for usage of these larger sized gratings in astronomical projects are reported. One application is meteor spectroscopy, where a Thorlabs grating (600 L/mm) is used in connection with a fisheye lens [12]. Another example is a recent test of the same grating type in connection with a telephoto lens and a DSLR camera [8]. However, no studies are known focusing on the optimization of resolution.

This report will show, that results can be obtained for a wide range of targets, which are comparable to those of much more expensive slit spectrographs. Having this in mind the absence of a widespread use of transmission gratings in the amateur scene is amazing. Only one can speculate about the reasons. Perhaps, the bad reputation of slit-less spectroscopy bears the blame. In contrast to slit spectrographs, it is often considered as "dirty", contaminated with several artefacts, strongly seeing-dependent and not reliably reproducible. Indeed, more care has to be taken compared to slit-based solutions. But valuable results can definitively be gained with some experience and understanding of the basics behind this technique. For example, one of the most annoying drawbacks, the disturbance by 0th order images, can easily be eliminated by simple constructive means, as is shown in section 3.

The main disadvantage is probably associated with absolute wavelength calibration. In contrast to slit spectrographs, there is no unambiguous relation between the sensor's pixel position and wavelength. Therefore, spectra have to be calibrated individually by stellar lines (relative calibration). For wavelengths above 6000 Å, however, often an exact absolute calibration is possible by using the telluric lines of O_2 and H_2O molecules.

Objective grating spectroscopy is further facilitated by the fact, that only rather small telescopes - and therefore small mountings - are required and that even guiding is often unnecessary. A wide range of imaging optics might be used, preferably apochromatic refractors. A b/w imaging camera should be chosen with appropriate small pixels, matched to the focal length and seeing condition to assure proper sampling.

2. Theory

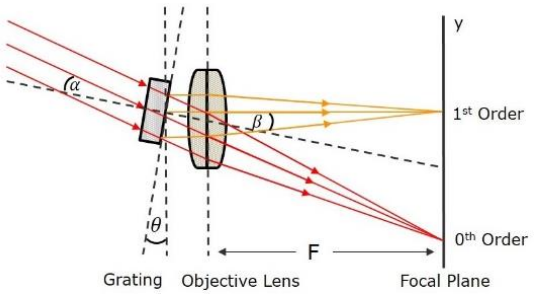

Fig. 1: Principle of the objective grating setup. The angles α, β and Θ are explained in the text.

Fig. 1 shows a transmission grating in front of an objective. In this general case, the grating plane is tilted against the optical axis by an angle Θ. The light from a star enters the transmis-

sion grating from the left under an angle of incidence α measured with respect to the grating normal. The 1st order deflection occurs under the angle β, which comes close to the tilt angle Θ. Because of the high dispersion the 0th order with deflection angle β = -α is normally far off the sensor for such configurations. Then, only a part of the 1st order spectrum is recorded, the size depending on the focal length *F* and the sensor dimensions. The relation between a small increment in deflection angle β and the corresponding linear distance on the chip is shown in fig. 2.

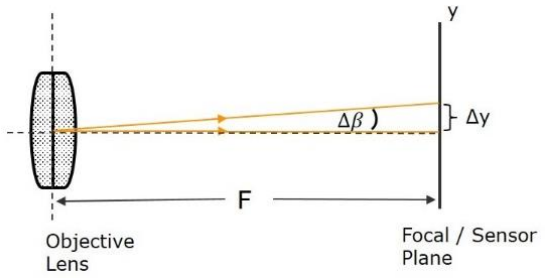

Fig. 2: Relation between the deflection angle increment Δβ and the corresponding linear extension on chip Δ*y*.

From grating theory, we get

$$\sin\alpha + sin\,\beta = n\,\frac{\lambda}{g} \qquad (1)$$

where α is the incident angle, β the deflection angle, *n* the diffraction order, λ the wavelength and *g* the grating constant.

Only the first order is considered from now on, thus *n* = 1. To calculate the angular dispersion, we write equation (1) in differential form

$$\mathrm{d}\alpha\,\cos\alpha + d\beta\,cos\,\beta = \frac{1}{g}\;d\lambda \qquad (2)$$

The incident angle α is defined by the star's position for a specific measurement and is fixed for this reason, thus dα = 0. Therefore, from (2) we get the angular dispersion (note, β is given in radians)

$$\frac{d\beta}{d\lambda} = \frac{1}{g\,cos\,\beta} \qquad (3)$$

Looking at fig. 2 and considering the fact that the sensor size is much smaller than the focal length we arrive at the approximation
$\Delta y \approx \Delta\beta \cdot F.$
With
$d\beta = dy\,/\,F$
the linear dispersion becomes

$$\frac{dy}{d\lambda} = \frac{F}{g\,cos\,\beta} \qquad (4)$$

For practical reasons, the reciprocal linear dispersion is used more often. It is typically expressed in [Å/mm] or [Å/Pixel] and is simply the inverse of (4)

$$\frac{d\lambda}{dy} = \frac{g\cos\beta}{F} \qquad (5)$$

In a next step, we will first consider the "standard case" of a grating perpendicular to the optical axis for simplicity, thus Θ = 0 and β ≈ 0. Using the first two terms of the Taylor series expansion for cosβ, (5) can be approximated for small angles β with high accuracy by

$$\frac{d\lambda}{dy} = \frac{g}{F}\left(1 - \frac{\beta^2}{2}\right) \qquad (6)$$

For a beam exactly on the optical axis (β = 0) we get the reciprocal dispersion

$$\left.\frac{d\lambda}{dy}\right|_0 = \frac{g}{F} \qquad (7)$$

From (7) the value covered by one sensor pixel can directly be calculated by

$$\Delta\lambda_{Pixel} = \frac{d\lambda}{dy}\,\Delta y_{Pixel} = \frac{g}{F}\,\Delta y_{Pixel} \qquad (8)$$

It is often convenient to switch to practical units

$$g\;[m] = \frac{10^{-3}}{L_{mm}} \qquad (9)$$

$$F\;[m] = 10^{-3}\;F_{mm} \qquad (10)$$

where the grating constant is given in lines per mm value and the focal length in mm.

The corresponding wavelength interval for one pixel in Ångstrom units is

$$\Delta\lambda_{Pixel}\,[\text{Å}] = \frac{10^4}{L_{mm}\cdot F_{mm}}\;\Delta y_{Pixel}\,[\mu m] \qquad (11)$$

with $\Delta\lambda_{Pixel}$ [µm] is the pixel extension along the dispersion direction measured in µm.

As an example, we consider a 300 L/mm grating together with the ATIK One (pixel size 4.54 µm) operated at a focal length of 500 mm. This yields a (reciprocal) dispersion of 0.327 Å/pix. Please remind that this calculation is valid only at β ≈ 0 for a configuration with the grating's plane perpendicular to the optical axis (parallel to the objective). For a grating tilted with respect to the objective plane (Θ ≠ 0) an

additional factor of cosβ has to be applied according to eq. 5. For the following discussion, the optical axis results (7), (8), (11) are of sufficient accuracy and therefore will be used in the next derivations for simplicity.

Because we are using a slit-less configuration, the spectrograph's resolution depends on the recorded image size of our object. If we assume a point like object, i.e. a star, its linear extension (characterized by e.g. the full width at half maximum (FWHM) of the point spread function on the sensor) may be denoted as ΔS_y. Sources of this blur are discussed below in detail. More precisely, this value is often related to the width of the "Line Spread Function" (LSF) in the literature since only the extension in dispersion direction is of relevance. The corresponding wavelength uncertainty ΔS_λ can be expressed as

$$\Delta S_\lambda = \frac{d\lambda}{dy}\,\Delta S_y \qquad (12)$$

The linear extension ΔS_y is given by the product of its angular dimension in radian measure and the focal length, hence

$$\Delta S_y = F\,\Delta\hat{S}_y \qquad (13)$$

together with (7) and (12) we have

$$\Delta S_\lambda = g\,\Delta\hat{S}_y \qquad (14)$$

Let's again switch to more practical units

$$\Delta\hat{S}_y = 4{,}848\cdot 10^{-6}\,\Delta S_y^{"} \qquad (15)$$

$$\Delta S_\lambda = 10^{-10}\,\Delta S_{\text{Å}} \qquad (16)$$

where $\Delta\hat{S}_y$ is in radian measure, $\Delta S_y^{"}$ in arc seconds and ΔS_λ in m.
Putting (9), (14), (15) and (16) together, we finally get the wavelength blur in Ångstrom units

$$\Delta S_{\text{Å}} = 48{,}48\cdot\frac{\Delta S_y^{"}}{L_{mm}} \qquad (17)$$

It is remarkable, that – besides the star's size - the theoretical uncertainty of wavelength and thus the resolution only depends on the grating used. Especially, there is no explicit dependency on the focal length. However, one has to keep in mind, that these considerations demand the use of appropriate sensors to fulfil sampling requirements, which is discussed in more detail below.

There are several contributions to the star's size $\Delta S_y^{"}$, some are under control by the observer, while others are fixed to the setup or depend on the observing conditions. Usually, the main contributions - which belong to the second class - are:

- $\Delta S^{"}_{Aperture}$: The diffraction pattern according to the form and size of the grating illuminated and
- $\Delta S^{"}_{Seeing}$: The widening due to air turbulences (scintillation).

Several other effects may be of importance resulting in additional unsharpness:

- $\Delta S^{"}_{Guiding}$: Improper guiding or mount alignment and
- $\Delta S^{"}_{Stacking}$: Stacking flaws during image preprocessing.

The image may be further distorted due to imperfect optics or focusing, also temperature drifts might be an issue. Since all these effects can be considered as statistically independent, they add quadratically to the final image size

$$\left(\Delta S_y^{"}\right)^2 = \left(\Delta S^{"}_{Aperture}\right)^2 + \left(\Delta S^{"}_{Seeing}\right)^2 + \left(\Delta S^{"}_{Guiding}\right)^2 + \left(\Delta S^{"}_{Stacking}\right)^2 + \cdots \qquad (18)$$

In (18) the contribution from the diffraction pattern, $\Delta S^{"}_{Aperture}$ is constant for a specific wavelength and grating. The rectangular grating produces the same diffraction pattern as a slit with width *D*, where *D* is measured along the grating's dispersion direction. Especially for large incident angles α, this width is effectively shortened by a factor of cosα, because the incident beam "sees" only this grating extension due to projection effect. Thus, we have

$$D_{eff} = D\cdot\cos\alpha \qquad (19)$$

For further estimations, we use the Rayleigh criterion applied to diffraction at the slit for further estimation. Here, two lines are considered as separated, when the 0th order maximum of one line coincides with the first diffraction minimum of the second line. In radian measures this leads to

$$\Delta\hat{S}_{Aperture} = \Delta\hat{S}_{Slit} = \frac{\lambda}{D_{eff}} \qquad (20)$$

Converting to arc seconds with eq. 15, one can note in practical units

$$\Delta S^{"}_{Aperture} = \frac{114"}{D_{eff}[\text{mm}]}\cdot\frac{\lambda_{nm}}{550\ [\text{nm}]} = \frac{114"}{D\ [\text{mm}]\cdot\cos\alpha}\cdot\frac{\lambda_{nm}}{550\ [\text{nm}]} \qquad (21)$$

When applying this relation to a grating with width 5 cm, one gets
$\Delta S^{"}_{Aperture} \approx 2.3"$
at 550 nm for small values of α, where $D = D_{eff}$. The resolution varies with wavelength leading to e.g. 1.7” at 400 nm and 3.3” at 800 nm.

The next important contribution to the spectral line blur is the seeing, which is varying over time and depends on the air mass and the observing site. At my location $\Delta S^{"}_{Seeing}$ typically ranges from 2” to 3” for stars higher than about 30° above the horizon.

Further contributions like $\Delta S^{"}_{Guiding}$ and $\Delta S^{"}_{Stacking}$ can principally be minimized by a careful observational setup and processing. Values well below 2” are reachable and should be aimed at. In total typical observed star sizes at 550 nm are $\Delta S^{"}_{y} = 3" - 5"$.

Fig. 3 shows the absolute resolution dependence on seeing conditions for the specific wavelength of 550 nm. Note, that the calculations are based on (17), (18) and (21), for a grating parallel to the objective lens, Θ = 0. Only the most important contributions $\Delta S^{"}_{Aperture}$ and $\Delta S^{"}_{Seeing}$ are considered. From the figure only a moderate influence of the seeing can be deduced. Being more precise for an increase of seeing of 10% at 3” the resolution of the 600 L/mm grating is degraded by about 6%.

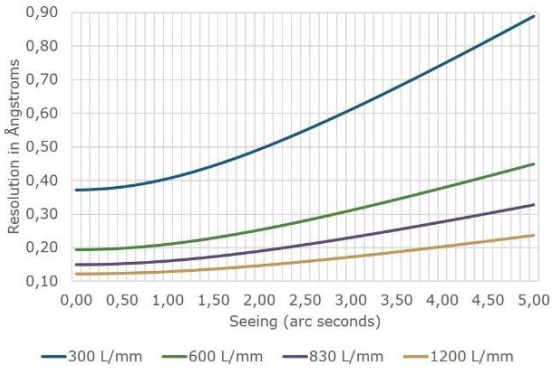

Fig. 3: Calculated absolute resolution as a function of seeing condition for a wavelength of 550 nm for a grating parallel to the objective lens, Θ = 0 (only contributions $\Delta S^{"}_{Aperture}$ and $\Delta S^{"}_{Seeing}$ included).

Fig. 4 illustrates the dependence of the resolution from the wavelength at a constant seeing of 3”. As above, the calculation for a grating with D = 50mm are based on (17), (18) and (21), regarding only the contributions $\Delta S^{"}_{Aperture}$ and $\Delta S^{"}_{Seeing}$. The respective incident angle α has been calculated using the grating equation (1). Especially for the 1200 L/mm grating curve, a progressive degradation of the resolution can be observed towards the red end. This is a consequence of the large incident angle α, leading to an enlarged diffraction pattern due to a significantly reduced D_{eff}, according to (19) and (20). This effect can be reduced by tilting the grating instead of using it parallel in front of the objective. This kind of optimization is discussed in section 4.

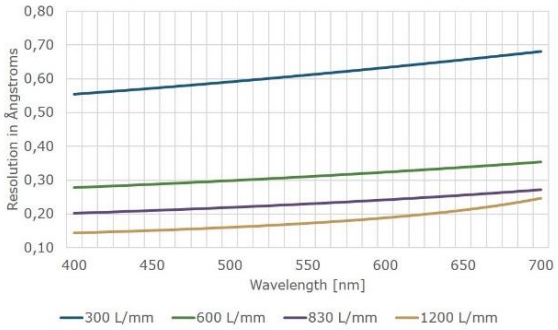

Fig. 4: Calculated absolute resolution as a function of wavelength for constant seeing of 3” (only contributions $\Delta S^{"}_{Aperture}$ and $\Delta S^{"}_{Seeing}$ included), Θ = 0

Now we want to compare the above findings with the restrictions on resolution imposed from diffraction grating theory. The latter states that the maximum possible relative resolution is given by

$$R = \frac{\Delta\lambda}{\lambda} = N \qquad (22)$$

where N is the number of grating lines illuminated by the beam. The maximum resolution calculated this way for the 5x5 cm² gratings is shown in tab. 1.

G [L/mm]	TR5	Measured optimum resolution at Na-D 589 nm		RD [Å/pix]	OWI [Å]
		FWHM [Å]	*MR*		
300	15,000	0.70	8,400	0.30	831
600	30,000	0.35	16,900	0.15	413
830	41,500	0.30	20,000	0.11	294
1200	60,000	0.19	31,000	0.075	205

Tab. 1: Maximum achievable resolution and measured optimum resolution as well as further parameters for the applied gratings. Equipment used: 80/500 mm ED refractor and ATIK One camera. G…grating, TR5…theoretical resolution of fully illuminated 5 cm grating, FWHM … full width at half maximum of sharpest lines in spectrum, MR…measured resolution, RD… Reciprocal Dispersion, OWI…Overall wavelength interval on the chip.

When looking at fig. 3, one can see that even for zero seeing (“outside the atmosphere”) the resolution doesn’t reach the theoretical limits presented in tab. 1. For e.g. the 600 L/mm value

shows a minimum of 0.194 Å at 5,500 Å, thus R = 28,350. In practical situations, the reachable resolution is further reduced. In anticipation of the next section tab. 1 contains measured resolution values, which are about half the theoretical limits.

When performing spectroscopic measurement, care has to be taken to use sufficient sampling. Since a detector pixel averages the flux over a specific wavelength interval, there may be a severe decrease of resolution, if the sampling is too coarse. In fact, the final star size according to (18) should span enough pixels on the sensor. The question is, how much is "enough". While it is rather clear intuitively, that less than 2 pixels per FWHM are not appropriate to reconstruct a spectral line, there is still some discussion about optimum sampling in the literature [13], [14]. For today's professional work, values between about 3 and 6 seem to be in practical use.

When looking at a typical configuration used in this work, we have the ATIK One camera operated at a focal length of 500 mm. This results in an angle of 1.87" per sensor pixel. With the above estimation for usual seeing conditions and a resulting $\Delta S_y^{"} = 3" - 5"$ we would have about 1.6 to 2.7 pixels covering the star's image. This means that for medium to bad seeing conditions the sampling seems to be just acceptable, while for good seeing definitively undersampling occurs. Especially in the latter case longer focal lengths should lead to an increase of resolution, which was indeed observed in practice. On the other hand, there is always a trade-off between resolution and the covered wavelength region.

3. Tests and experiences with different setups

3.1 First tests with "Star Analysers" from Paton Hawksley, need of blockers and aperture stops

For owners of the well-known Star Analyser transmission gratings it is rather tempting to put such a device in front of a telephoto lens or a small refractor. Mounting aids can either be self-made or be ordered from suppliers, e.g. ref. 7. A typical spectrum produced in this way is shown below. A Star Analyser 200 (SA200) was mounted in front of a 60/330 mm ED refractor with the effective focal length reduced to 210 mm. An ATIK One with 4.54 µm pixels was applied as the imaging camera. The resulting dispersion has been measured to 1.09 Å per pixel, in good agreement with (11). 18 exposures of 30 s were stacked. Besides the dominant Balmer lines many spectral details are visible, the Na-D lines are clearly resolved. The measured absolute resolution Δλ is better than 3 Å.

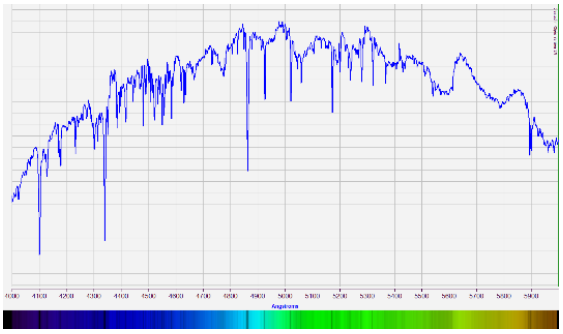

Fig. 5: Raw spectrum profile of Deneb from 400 to 600 nm, 9.9.2015, SA200 in front of ED 60/330 mm refractor.

The following summarizes my experiences with such setups.

The main restriction is the small size of the grating. The diameter is only about 24 mm.

1) The effective aperture of the optics used is reduced to "one inch". Therefore, only bright targets are in reach with moderate exposure time, if one wants to have reasonable statistics. In addition, a sensitive b/w camera with small pixels is highly recommended.
2) The resolution is mainly limited by the large size of the Airy disk of nearly 6" in this case. From (17) a maximum possible resolution of about 1.5 Å could be expected. This value is not reached in the above-mentioned setup mainly because of undersampling. The resolution can be enhanced in some way by using a larger focal length or a sensor with smaller pixels.

The main advantages are:

1) The low cost and the very simple setup, which is ideal for testing and getting familiar with this technique.
2) Usually, any optics used is stopped down to a large extent resulting typically in an improved performance. Especially the chromatic errors are reduced. Therefore, a variety of optics may be usable in such configurations, e.g. Fraunhofer achromats.
3) Since the star size is dominated by the Airy disk, there is only a very small sensitivity to seeing conditions.

A principal problem for objective grating configurations can be illustrated by the 2-D image of the above Deneb spectrum. In fig. 6 one can see, that the whole image is crowded with more

or less intense 0th order images of stars in the current field of view.

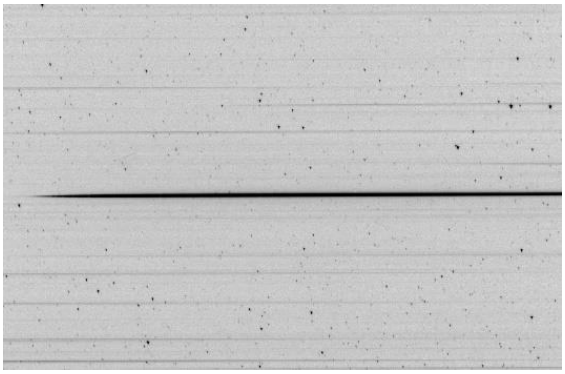

Fig. 6: Negative raw image of the Deneb spectrum from fig. 5.

It is obvious, that such “contaminations” will affect the derived spectrum’s quality. If 0th order images are located in the spectrum’s integration region, they will produce artificial „emission lines”. Those ones located in the background subtraction regions will show up as additional “absorption lines”.

Fortunately, this problem can easily be addressed by simple measures. Fig. 7 shows a “beam blocker” construction made of cardboard and tailored for the specific optics. The direct beam on the optical axis producing the crowded 0th order images is simply blocked. The incoming rays for the 1st order can still reach the grating. For alignment and mount initialization purposes the blocker is equipped with a removable cap.

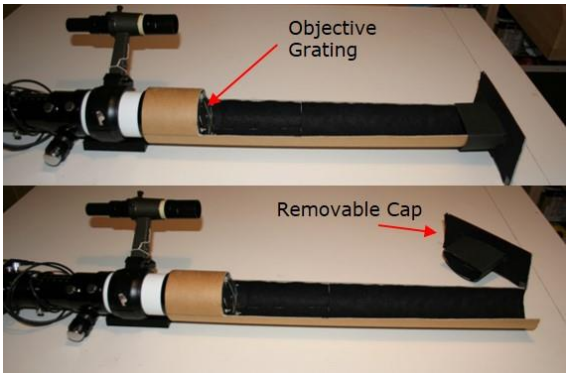

Fig. 7: “Beam blocker“ in front of 60/330 mm ED refractor for suppressing 0th order images

When using the 5x5 cm² gratings, the effective area is about five times as large compared with the Star Analyser. Thus, even fainter objects are now in reach for spectroscopy. Unfortunately, the whole grating area could mostly not be used for the gratings tested throughout this work. The spectrum shows some distortions, as can be seen in fig. 8 for the case of the 1200 L/mm grating. This is probably due to imperfect manufacturing quality not suppling straight grooves over the whole grating area. When adding an aperture stop of 5x2.5 cm², the spectrum is of much better quality. The spectral lines become sharper and the spectrum’s height is reduced. The size and position of the aperture stops had to be worked out individually for each grating by trial and error. The 600 L/mm grating gave reasonable results without stops. For the 300 L/mm and 830 L/mm gratings stops of 5x4 cm² and 5x3 cm², respectively, were applied.

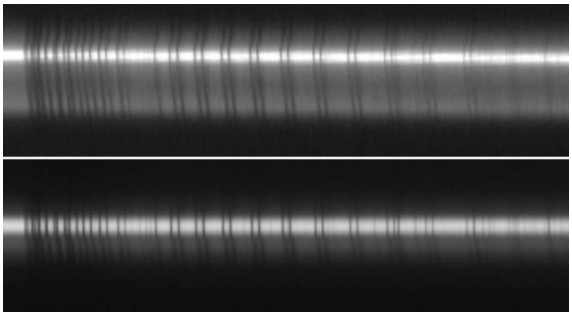

Fig. 8: 2-D 1200 L/mm grating O_2 A-band spectral image without (top) and with a 5x2.5 cm² aperture stop (bottom).

3.2 The 300 L/mm 5x5 cm² grating from Thorlabs

This grating turned out to be a “general-purpose device” for medium resolutions up to about *R* = 8,000. The applied aperture stop was 5x4 cm². Compared to the higher dispersion gratings, it provides the easiest handling. For most parts of the visible spectrum, the efficiency is quite high, with peak values around 75% according to Thorlabs fig. 9 [11].

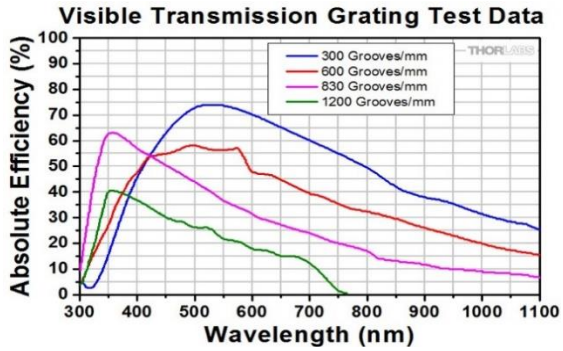

Fig. 9: Grating efficiency for visually ruled gratings (Source: Thorlabs Inc.)

Thus, the grating can be applied from the near UV to the near IR region. The quite small deviation angles from 6° at 350 nm to 14° at 800 nm makes positioning rather easy. Together with

the moderate dispersion, rather large wavelength areas up to around 100 nm may be covered, suitable for overview purposes. This is demonstrated in fig. 10, where a spectrum from Deneb's Hα region is shown. In this case, the grating has been applied to an 80/500 mm ED refractor, with a reduced focal length of 434 mm. 22 exposures with 30 s each were stacked. The absolute resolution was slightly below 1 Å in this case, enough for displaying details of Deneb's Hα profile. The wavelength spans from the O_2 band at 628 nm to the B-band at 687 nm. Together with further H_2O lines around Hα, these lines provide a very accurate basis for an absolute telluric wavelength calibration.

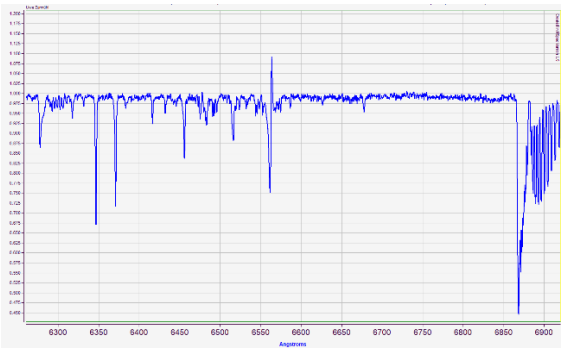

Fig. 10: 300 L/mm grating rectified spectrum of Deneb around Hα, 7.5.2016

Remark on 2nd order spectrum

For deviation angles higher than about 13°, the second order may overlap with the first one. This grating still has a quite high efficiency for the 2nd order in the blue region. Therefore, in case of spectroscopy in the near IR region, an appropriate lowpass filter has to be applied, for e.g. an orange or red edge filter. An interesting alternative setup also may consist in adding a prism in front of the sensor, with dispersion perpendicular to the grating's dispersion. In this way, a part of the IR spectrum and near UV / blue spectrum may be measured simultaneously. An example for this technique is shown in fig. 11. In this case, a wedge prism with 2° deviation angle mounted in a 1,25" filter set has been put 5 cm in front of the CCD sensor.

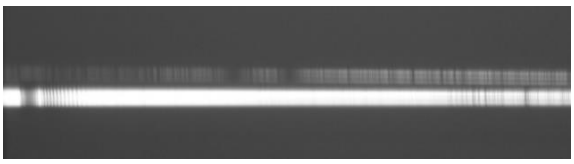

Fig. 11: Spectral image of Arcturus, with simultaneous recording of H&K region (top) and near IR above telluric A-band (bottom)

In this way, the second order allows to record spectra for bright stars with doubled resolution from wavelengths around 360 nm up to about 500 nm.

3.3 The 600 L/mm 5x5 cm² grating from Thorlabs

For higher resolutions up to about R = 16,000 this grating may be applied. Because of its higher dispersion and lower efficiency compared to the 300 L/mm grating only brighter targets are accessible and the exposure time has to be enlarged. In addition, the deviation angle gets a little bit more unhandy, with 12.1° for 350 nm and 28.7° at 800 nm. No aperture stop had to be applied for this grating.

The sample spectrum in fig. 12 shows the interesting Hα line of ε Aurigae, with its characteristic absorption and emission profile, the "red" and "blue" horns. Those structures are worthwhile to monitor, since they show drastic variations over different time scales. For the spectrum 33 exposures of 60 s were stacked. The objective lens was a 60/330 mm ED refractor, giving a dispersion of 0.225 Å/pix. The measured resolution (R = 12,000) was below the grating's optimum value, mostly due to undersampling.

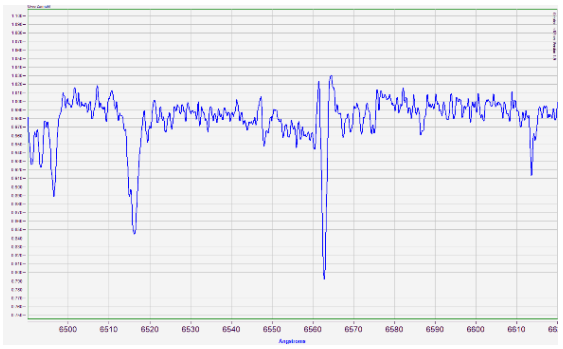

Fig. 12: 600 L/mm grating rectified spectrum of ε Aurigae around Hα, 16.12.2016

3.4 The 830 L/mm and 1200 L/mm 5x5 cm² gratings from Thorlabs

When the highest resolutions are demanded, these gratings come into play. With deviation angles at Hα of 33° and 52° respectively, the operation becomes more complicated. The gratings have to be well aligned in - favorably - north-south direction with respect to the dispersion. Only then it is an easy task to find the star's spectrum at such a distant sky position. Because of the dimmer spectra, focusing also becomes a challenge. This topic will be discussed in the next section. The applied aperture

stops were 5x3 cm² and 5x2.5 cm², respectively.

Once everything is set up correctly, high resolutions are accessible, resulting in detailed spectra. This is demonstrated by the spectrum of the Be / shell star ζ Tauri in fig. 13. The Hα emission peak shows a sharp central absorption. This feature shows strong variations over time, depending on the orientation of the surrounding gas disk with respect to the observer. For this spectrum, 62 single exposures of 30 s were stacked. The measured resolution was about 17,000.

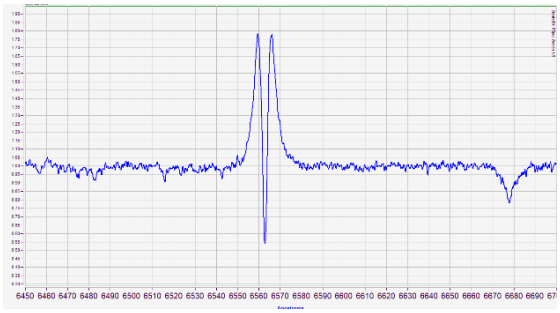

Fig. 13: 830 L/mm rectified spectrum of Be star ζ Tauri around Hα, 16.12.2016

For rather short wavelengths, in the near UV and violet region, the efficiency of these high dispersion gratings is comparable with the 300 L/mm grating (refer to fig. 9). This allows for a high-resolution study of the Ca II H&K lines. These very broad photospheric absorption lines exhibit rather sharp chromospheric emission cores with central absorption for late type stars. According to O.C. Wilson and M.K. Vainu Bappu the strength of the emission is directly related to the absolute magnitude of the star, thus providing an independent measure for the star's distance [15].

The spectrum in fig. 14 shows a measurement of the K0III star Arcturus. 77 exposures of 60 s were stacked. A 120/900 mm ED refractor was used. This yielded a dispersion of 0.0394 Å/pix for the ATIK camera sensor. The measured resolution was about 0.18 Å or R = 22,000 at these wavelengths.

The medium wavelength spectrum of fig. 15 was measured with the focus on optimizing resolution. The seeing conditions were good with the target standing more than 50° above the horizon. By the aid of a Barlow lens, the focal length of the 80/500 mm ED refractor was extended to 1374 mm, yielding a dispersion of 0.027 Å/pix. In this way, a more than enough sampling could be guaranteed (about 6 pixels per FWHM). The effort did payoff: The absolute resolution of about $\Delta\lambda$ = 0.17 Å (R = 30,000 at 5,170 Å) was the best one recorded so far with such configurations. In total 3,270 s of exposure time were summed up for this spectrum. The Mg triplet is resolved in great detail, with a lot of satellite components and interspersed spectral lines.

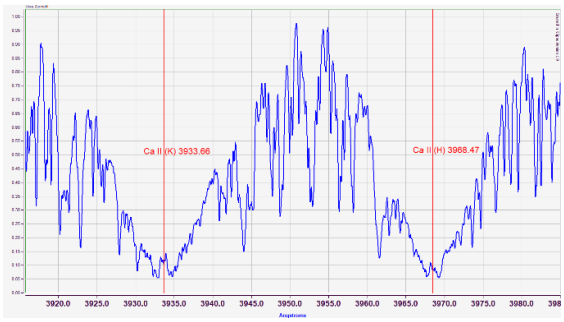

Fig. 14: 1200 L/mm rectified spectrum of Arcturus, showing the Wilson-Bappu effect of the CaII H&K lines, 18.4.2018

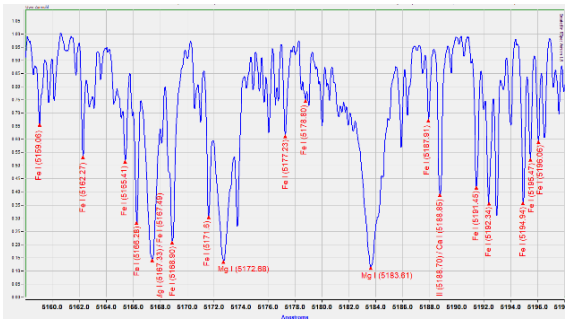

Fig. 15: 1200 L/mm rectified spectrum of Arcturus, showing the Mg triplet region, 21.4.2018

4. General remarks on current setups and possibilities for optimization

"Prototype phase"

With respect to the results presented in this paper, it must be noted, that these experiments are still in a certain kind of prototype stage. Especially, it is not clear, if the four gratings from Thorlabs represent typical samples or other gratings from a different manufacturing processes or other suppliers behave similar. There are still some unclear effects, which are not understood and need further measurements and tests.

Optical system used

A variety of usual amateur optics can be applied as long as the quality is appropriate ("diffraction limited"). A positive side-effect of the limited grating size is the "slowing down" of most optics. For example, a 100 mm f/7 refractor will be stopped down to a 50 mm f/14 system, when a 5x5 cm² grating is applied in front of it. This nor-

mally reduces the residual aberrations significantly, especially the chromatic aberration. Therefore, also high quality Fraunhofer lenses may be applied. Apochromatic refractors have the advantage of a constant focus over a wide wavelength interval, so fewer re-focusing is necessary. Especially for near UV measurements, Newtonians have been used with success. A principal drawback may consist in the partial obstruction of the grating caused by the secondary mirror.

The focal length should always be chosen in accordance with the sensor's pixel size for appropriate sampling, as discussed at the end of section 2. For the used ATIK One, favorable focal lengths are in the range from about 500 to 1000 mm.

Sensors / cameras used
In the present work, mainly the ATIK One camera has been used. The camera is identical to the ATIK 460EXM camera, except for the additional filter wheel. Both cameras are based on the Sony ICX694ALG CCD sensor, with a size of about 12.5x10 mm² and 4.54 µm pixels [16]. Imaging systems based on this chip are commonly used for high resolution spectroscopy work, because of their excellent performance.

Besides this, a somewhat outdated Meade DSI3 camera has been used in the beginning. It features an ICX-285ALM CCD sensor, with a size of about 8.8x6.6 mm² and 6.45 µm pixels. Cameras using this chip can still be found quite regularly in spectroscopy projects, for e.g. the ATIK 314.

Some tests were performed with a CMOS camera, namely the ZWO ASI 178MMC, which offers the finest pixels (2.4 µm). Though very useful for deep sky imaging, this camera proved to be impractical for my high-resolution spectroscopic work. The reason was the occurrence of high frequency fringes showing up in the recorded spectra, most likely caused by interferences produced by sensor components themselves.

Focusing
As already noted above, the exact focusing may be a real challenge. With higher groove density the dispersion grows, leading to increasing dimmer spectra. In contrast to slit spectrographs, no focusing on artificial light sources is possible. Instead, the focus has to be adjusted using a real star. Bright stars with sharp spectral lines of high contrast are clearly recommended. For low to medium wavelengths, the G-band, Mg-triplet and Na-D lines of giant stars provide such structures, e.g. Capella and Arcturus. For longer wavelengths, the telluric B-band and A-band may be useful. In this case, any bright star like Vega or Deneb might be chosen. Even then focusing can be rather time-consuming, because a 1200 L/mm grating only begins to show enough details for exposures longer than about 10 s. In addition, the focus has to be re-checked regularly when changing the measured wavelength range significantly or after some hours of observation.

Guiding
The requirements on guiding are quite similar compared to those of deep sky imaging. Especially, it is essential to avoid short-period drifts of stars and to take countermeasures against the mount's right ascension periodic error and similar. It has to be kept in mind, that - in contrast to slit spectroscopy - every movement of the star's position in dispersion direction reduces the spectral resolution. From the latter it should be clear, that it is favorable to mount the grating with its dispersion in north-south direction. In this way, any residual periodic mount error only enlarges the spectrum's width but does not degrade the resolution.

When taking long exposures, normally guiding is necessary. On the other hand, many of the results presented in this paper were gained without guiding. This was achieved by a well aligned mount and rather short exposure times up to 60 s. Please note, that guiding is complicated or even impossible by the large incident angles for the high dispersion gratings, which may exceed 50° when measuring Hα with the 1200 L/mm grating (refer to fig. 16).

Handling of gratings & dew problem
In order to handle the gratings, self-made mounts cut out of plastic sheets were applied. Since the gratings have no protective layer and are mainly produced for applications in clean environments, great care has to be taken when handling. Like most other gratings used in spectroscopy, the surface must not be touched. Also, cleaning is not possible, just a gentle air stream may be applied for removing dust grains.

Another risk is the formation of dew on the grating, which might also lead to abrasion due to particles and chemicals contained in the atmosphere's water vapor. Besides this, even the first signs of dew will quickly result in a fading diffraction. A dew protection is therefore essential, it can easily by achieved by commercially available heaters for telescope tubes. When not in use, it is advisable to store the gratings in a dry and clean place.

Pre-processing / stacking

The pre-processing follows mainly the standard procedures known from deep sky imaging. For this report, mainly the program “Astroart 6” [17] was applied, but a variety of similar programs might also do a good job. First, the single exposures of a measuring set are added (“stacked”), thereby correcting a possible shift between the single images. In addition, a dark field is subtracted, sensor pixel defects and cosmic ray traces are eliminated. For the latter, Astroart offers specific features and a sigma-clipping method for summation. For spectroscopic images, Astroart has a specific automatic alignment method, which works quite well in case of strong absorption lines. In case of weak absorption lines or sharp emission features, I made the best experiences with the “manual” stacking method. For images which are critically sampled, I apply the re-size option when stacking. With a 2x re-sizing I found the resolution in the sum image to be slightly enhanced. This effect somehow resembles the “dithering” procedure applied elsewhere in order to get sharper astronomical images. As a funny incidental remark, the above methods show an advantage of slitless spectroscopy. Because the spectral lines are drifting (very slowly!) over the sensor, different pixels are involved in the course of a typical measurement, making the elimination of defects easier. With slit spectroscopy, in contrast, the slit position is stable over a much longer time, with only the same set of pixels contributing to the spectrum.

The next steps are the rotation (horizontal alignment) of the spectrum and cropping the region of interest in order to conserve disc space. Further processing is done by using a program for extracting the 1-D image from this cropped raw 2-D image. I personally prefer RSpec for this task, because it is well suited for quick individual adjustments of the binning regions for slit-less spectroscopy [18].

Methods for background reduction

One of the main drawbacks in contrast to slit spectroscopy is the high background, originating from a diffusely illuminated sky. While this may not be an issue for bright stars in a rather dark sky, spectra of weaker stars normally will be simply lost in a hazy, moonlit night. There is, however, a countermeasure which can reduce this problem. For most cases, the spectral region covered by objective gratings is rather small, typically about 100 nm for low dispersion and much less for high dispersion setups. Therefore, specific filters can be applied. For e.g. when measuring Hα region and above, I usually apply an orange low-pass edge filter. The transmission in the measured region is still near 100%, but a great number of unwanted photons is blocked. For high dispersion work even the use of narrow band filters may be appropriate, thus reducing the background even much more. In other wavelengths regions standard RGB bandwidth filters also may be applicable. In addition, when measuring in the near IR region, low-pass filters are normally necessary to suppress the 2nd order. With filters, one should take care not to introduce fringing effects. This indeed was observed when using a specific edge filter. So, it is recommended to test any filter by recording a high S/N spectrum and looking for ripples in a smooth part of the continuum.

Wavelength calibration

Probably the severest drawback compared to slit spectrographs is the lack of a direct absolute wavelength calibration. On the other hand, a relative calibration is possible for most spectra by comparing the lines in the spectrum to a star of similar type and assigning the corresponding wavelengths. This task is supported by a variety of spectral atlases and digital wavelength tables. For many projects this relative calibration is completely sufficient.

When absolute calibration is needed, the atmospheric lines of O_2 and H_2O offer very precise wavelength standards above about 600 nm. For e.g. the O_2 telluric bands are listed in [19]. Furthermore, some interstellar lines may also be used for distant targets. Especially the Na-D lines provide an absolute measure, though not as precise as the telluric lines.

For objective gratings, calibration is simplified by the fact, that the dispersion is nearly linear. Thus, a linear fit to the used calibration lines normally gives a good approximation, while a quadratic fit is mostly perfect.

A strange effect:
The height of the objective spectra

While performing the first tests with the objective gratings presented above, it turned out that for the sharpest focus position all spectra were significantly different in height. Values from about 30” to 70” were measured (without aperture stops). These values only showed a very small dependence on the optics used, so the effect seems to be originating from the gratings themselves. This was an unexpected and somehow disturbing finding. These relative broad spectra have the drawback of decreased intensity (per pixel) and spatial resolution, the latter restricting the use for double star spectroscopy. When applying the above described aperture stops, the height could slightly be reduced (by a factor of about 2/3).

The origin of this effect is currently unclear, perhaps there is some astigmatism introduced by bended surfaces due to the manufacturing process. It would be useful to test a larger quantity of gratings for further investigation.

Optimisation: Tilted grating, Θ>0

As discussed above, a grating mounted parallel in front of the objective lens is not ideal for large incident angles α. First, there is a reduction in intensity, according to the reduced effective grating size, $D_{eff} = D \cdot \cos\alpha$. Secondly, for the same reason the diffraction pattern is enlarged, leading to a degradation of resolution (refer to equation (19) and (20)). A simple countermeasure consists of tilting the grating. Fig. 16 shows the strong decrease in beam deflection for the 1200 L/mm grating. For Hα, the deflection is reduced from about 52° for zero tilt, Θ = 0, to 46.5° at Θ = 26°.

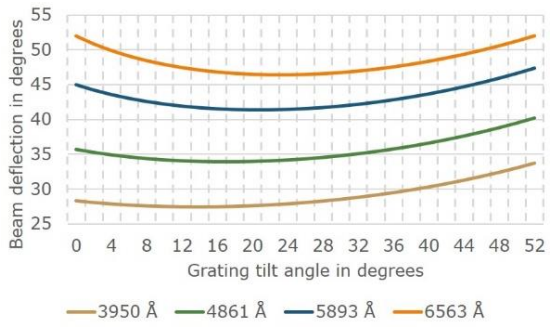

Fig. 16: Calculated deflection for 1200 L/mm grating as a function of tilt angle Θ for different wavelengths.

In practice, there is a little bit more effort when constructing a tilted grating setup compared to the parallel case. Something like a "grating wedge" has to be implemented. Fig. 17 shows an example made of cardboard for usage in front of a 102/714 mm APO refractor.

Fig. 17: Objective grating wedge for a tilt angle of 12°.

5. Summary & conclusion

In this report, I tried to give an overview and share my experience in the quite exciting and rather new field of objective grating spectroscopy for amateurs. The above treatment is far from being complete leaving much room for further investigations.
The sample spectra in this paper only give a first impression for possible projects. Many more objects are in reach, especially all sufficiently bright targets - stars brighter than about 6th magnitude where absolute wavelength calibration is either not necessary or can be achieved by telluric calibration.

Some examples are:

- Monitoring of Hα line profiles of supergiants (e.g. Deneb, Rigel),
- Be stars (e.g. γ Cas),
- Spectral fine structure in pulsating variable stars, like Mira,
- RV measurements, mainly on double stars,
- Bright transient phenomena (especially novae) and
- Eclipsing binary systems like Algol, VV Cephei and ε Aurigae

In fact, especially with the 300 L/mm grating spectra had been recorded for the amateur Algol Hα campaign lead by Bernd Bitnar [20].

The gratings used so far offer a way to a "Low cost / high resolution spectroscopy" for all amateurs equipped with some basic deep sky equipment, seeking a rather uncomplicated access to spectroscopy.

When looking at the presently available gratings, there is obviously a tradeoff between quality and cost. It would be fine to have gratings where the whole active area is useable, and which have reduced astigmatism. In addition, larger gratings would be very useful. For instance, an 8x8 cm² grating with full aperture could provide more than five times the intensity compared with the 1200 L/mm grating stopped down to 5x2.5 cm². But of course, such gratings still must be affordable. But even for those "small" gratings presented in this report I see a great future potential.

References

[1] U. Zurmühl, Spektrum 51 (2016) 10
[2] R. Riekher, Der Briefwechsel Joseph von Fraunhofers, Band 1, Akademische Verlagsanstalt, 2017, pp. 242-243, 316 and 320
[3] W.C. Seitter, Bonner Spectral Atlas I, Ferd. Dümmlers Verlag, 1970, Bonn

[4] W.C. Seitter, Bonner Spectral Atlas II, Ferd. Dümmlers Verlag, 1975, Bonn
[5] M. Wolf, Astron. Nachrichten 213 (1921) 50
[6] M. Köbberling, Sterne und Weltraum 6 (1998) 537
[7] Paton Hawksley Education Ltd., http://www.patonhawksley.co.uk/astronomicalgratings.html
[8] E. Wischnewski, Astronomie in Theorie und Praxis, 8. Auflage, 2018, p. 254
[9] R. Leadbeater, http://www.threehillsobservatory.co.uk/astro/astro.htm
[10] Chr. Buil, http://astrosurf.com/buil/index.html
[11] Thorlabs Website, grating section: https://www.thorlabs.de/
[12] M. Dubs and P. Schlatter, WGN Journal 43:4 (2015) 94
[13] J. G. Robertson, PASA 34 (2017) e035
[14] T. Eversberg and K. Vollmann, Spectroscopic Instrumentation, Springer-Verlag, 2015, Berlin, Heidelberg, pp. 72
[15] O. C. Wilson and M. K. Vainu Bappu, Astrophys. Jour. 125 (1957) 661
[16] ATIK: https://www.atik-cameras.com/
[17] Astroart: http://www.msb-astroart.com/default.htm
[18] RSpec: http://www.rspec-astro.com/
[19] H. D. Babcock and L. Herzberg, Astrophys. Jour. 108 (1948) 167
[20] B. Bitnar et al., this issue of Spektrum

Uwe Zurmühl had a strong interest in astronomy since his days of youth, observing sunspots and planets with a 40 mm refractor at the age of 12. He studied physics at the University of Göttingen, where he received his Ph.D. in 1983. After some years of research in medium energy physics, he has worked in the industry in the field of software engineering. Since 2015 his astronomical activities are focused on spectroscopy, mainly on investigating the application of transmission gratings.

A study of circumstellar material in β Persei

Bernd Bitnar[+], Christian Brock[++], Ulrich Waldschläger[o], Uwe Zurmühl[oo]
[+] Heinrich-Heine-Str. 2E, 01728 Bannewitz, Germany, Email: bernd.bitnar@gmx.de (Corresponding author)
[++] Sternwarte Gönnsdorf, Weißiger Landstraße 6, 01328 Dresden, Germany
[o] Am Schmeding 39, 12685 Berlin, Germany
[oo] Sandstraße 8a, 31180 Giesen, Germany

Abstract
The Hα profile of the eclipsing binary system β Per (Algol) shows a specific weak emission structure originating from circumstellar material flowing from the secondary to the primary star. To investigate the geometry of the circumstellar gas Hα spectra were taken over a five-year period between 2014 and 2019. A method to separate the weak emission profile from the dominating Hα photosphere absorption line was developed. The change of the emission profile as a function of the orbital phase was studied by applying this method to the observed spectra. The results were compared with a model of the circumstellar material from literature. By applying a velocity space analysis, the velocity coordinates of the dominating single peak emission structure were determined.

Zusammenfassung
Das Profil der Hα Linie des Bedeckungsveränderlichen β Per (Algol) weist eine spezifische schwache Emissionsstruktur auf, die durch zirkumstellares Material hervorgerufen wird, das vom Begleiter auf den Hauptstern fließt. Zur Untersuchung der Geometrie dieses zirkumstellaren Gases wurden Hα Spektren über einen Zeitraum von 5 Jahren von 2014 bis 2019 aufgenommen. Es wurde eine Methode entwickelt, die die Trennung des Emissionsprofils von der wesentlich stärkeren photosphärischen Hα Absorptionslinie erlaubt. Durch Anwendung dieser Methode auf die beobachteten Spektren wurde die Änderung des Emissionsprofils in Abhängigkeit der orbitalen Phase untersucht. Die Resultate wurden mit einem Modell des zirkumstellaren Gases aus der Literatur verglichen. Durch die Anwendung einer Analyse im Geschwindigkeitsraum konnten die Geschwindigkeitskoordinaten der dominanten Einzelpeak-Emission bestimmt werden.

Received: 2019-06-22, Revised: 2019-10-20, Accepted: 2019-11-11

1. Introduction

β Per (Algol) is the prototype of a binary system (Algol binaries), where the primary component is a hot main sequence star with a spectral type B5 – A5 and the secondary is a cool G – K subgiant filling its Roche lobe. Consequently, gas can flow from the secondary to the primary star. One distinguishes between slow and fast orbiting Algols. The slow orbiting systems show an orbital period of > 5 days and an accretion disc is formed around the primary. The fast orbiting Algols with a period of < 5 days form a disc-like structure, where the gas stream of the secondary is striking the surface of the primary star before performing a complete orbit [1].

Algol binaries show the Algol paradox: The more massive primary star is still on the main sequence, whereas the less massive secondary achieved already the red giant state. This paradox can be solved by the assumption that originally the secondary star was the more massive component, but it already lost most of his mass increasing the mass of the current primary star.

β Per is the brightest and closest Algol type binary. Much research was already carried out to investigate this prototype system in detail. The star is a hierarchical triple system with a close pair of a B8V primary with 3.4 M_{sun} and a K2IV secondary with 0.8 M_{sun} [2]. The almost circular orbit has a period of 2.87 days and an inclination of 98°, so partial eclipses occur. Due to its high brightness and its eclipses observable with the naked eye the system is the most popular occultation variable star. The orbital and the physical parameter of the components were determined by spectroscopy and by optical interferometry, as well [3].

A third component with spectral type F1V has a large orbit with a period of 1.9 years. The parallax of the β Per system is 35 mas [3], which corresponds to a distance from earth of 29 pc. The β Per binary shows a synchronized rotation. The rotational velocity of the primary $v \sin i$ is 53 km/s [1].

The circumstellar material due to the gas flow from the secondary to the primary can be detected by optical spectroscopy showing a weak emission embedded in the dominating photospheric Hα absorption line [4]. This emission was studied in detail by Richards et al. by evaluating spectra taken from 1972 – 1977 [1]. They found two separate emission components responsible for the total Hα emission: a strong, so called single peak emission, and a weaker double peak emission. A model of the circumstellar material contains a localized emission region, which correlates to the gas stream, and a disc-like region. This model will be described later in more detail. From the temporal coverage of the spectra a stability of the system over at least 43 days was found, but over longer time scales the system is variable.

In a later publication [5] the data from spectra from 1976 – 1977 were used to calculate a reconstructed 2D image of the emitting gas in velocity space, a so-called Doppler tomogram. This tomogram shows clearly the separate two emission regions found in the earlier paper. In the meantime, Doppler tomograms could be calculated for several more Algol type binaries [6].

In a recent study Richards et al. applied tomography techniques developed for radio astronomy applications to reconstruct a 3D tomogram of β Per [7]. Due to the slight tilt in inclination, gas flowing in *z* direction is resolvable in the spectra. It could be shown that the gas stream shows a significant velocity in *z* direction. The cause of this flow perpendicular to the orbital plane is assumed to be the magnetic field of the secondary. For this study spectra taken from 1992 Oct 06-21 were evaluated. β Per is also a radio and an X-ray source due to a magnetically active corona of the secondary star [8]. The system produces radio flares, which coincide with an enhanced Hα emission.

In this work the emission structure was investigated in detail by using new spectra taken between 2014 and 2019 with amateur equipment. One goal was the investigation on the quality of the data achieved considering the limitations of the small equipment used as well as of the modeling capabilities applied. A similar evaluation technique as described in [1] was developed. A second goal was a stability study of the emission structures found by Richards et al. on a longer time scale.

2. Experimental: Observation and reduction of Hα emission in spectra of β Per

The spectra were obtained from 3 observatories located in Bannewitz (near Dresden, Saxony), Berlin and Giesen (near Hildesheim, Lower Saxony). The observers used telescopes with apertures from 60 mm to 400 mm and different kind of spectrographs: a conventional grating spectrograph, an Echelle spectrograph and transmission gratings placed in front of the telescope aperture. Table 1 summarizes the equipment used.

Obs	Site	Telescope/ Spectrograph	Observing Period
BB	Bannewitz	C8 f/10 / LHiRes III 2400 l/mm	2014-09/2015
		RC 16” f/8 / LHiRes III 2400 l/mm	from 12/2015
UW	Berlin	LX200 10” f/10 / Czerny Turner 1200 l/mm	2015
		C14 f/10 / Echelle 79 l/mm, 63°	from 2017
UZ	Giesen	60/330 APO / 25 cm² objective grating, 600 l/mm	until 08/2017
		80/500 APO / 25 cm² objective grating, 300 l/mm	from 09/2017

Tab. 1: Telescopes and spectrographs used in this study. BB – Bernd Bitnar, UW – Ulrich Waldschläger, UZ – Uwe Zurmühl

Bannewitz used a LHiRes III spectrograph with a 2400 l/mm grating and a 23 µm and a 35 µm slit. The spectra were taken with a Σ 1603 CCD camera with 1.6 MPixel and 9x9 µm² pixel size. The spectral coverage with this setup for a typical Hα spectrum is the range from 6500 Å to 6650 Å with a resolution of 11000 - 17000. In Berlin most of the data were obtained with a self-built Echelle spectrograph [9]. The resolution is about 17000. The transmission grating technique applied in Giesen is described in detail in ref. 10. The resolution is about 7000. Data reduction including wavelength calibration was performed by the observers using individually chosen software tools. The atmospheric lines were removed with Spectrotools [11]. To ensure a high time resolution together with a high SNR the spectra were taken with 900 s exposure time, which corresponds to a phase resolution of 0.003 of the binary orbit.

A major challenge of the data evaluation procedure was the separation of the weak emission from the dominating Hα absorption line. For that purpose, a Python script was developed, which applies the following four evaluation steps:
1. By applying an orbital model for the 3 components of β Per the radial velocity of the primary for each observation date was calculated. Each spectrum was shifted to the frame of the primary. This means that the abscissa of each spectrum is the radial velocity of the Hα line relative to the rest frame of the primary.
2. From ref. 12 an atmospheric model of the Hα absorption line of the B8V primary was obtained and the model spectrum was shifted to the frame of the primary to compare it with the measured spectra. The photosphere input parameters of the primary were taken from ref. 1.
3. All spectra were normalized by fitting the experimental spectra to the model outside of the Hα absorption line.
4. By subtracting the model from the normalized spectra difference profiles were obtained showing the emission profile separated from the dominating photospheric Hα absorption. The detailed evaluation procedure is described in ref. 13. All these analysis steps were carried out centralized by a single data evaluator.

Figure 1 shows the evaluation result of a single spectrum. The measured raw spectrum (blue) is shown together with the model from [12] (green), both were shifted to the rest frame of the primary. By fitting the measured spectrum to the model outside of the Hα absorption line, the normalized spectrum (orange) is obtained. The difference of the normalized spectrum and the model gives the resulting difference profile (red). In this example, the difference profile shows two emission peaks, whose maximum positions are marked.

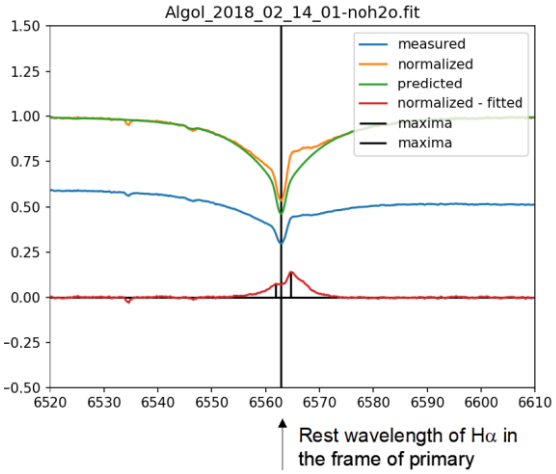

Fig. 1: Example for the evaluation steps of a single spectrum. The raw spectrum (blue) was taken at phase 0.38.

3. Results: Hα difference profiles from 2014 to 2019

From all measured spectra the difference profiles were calculated. Fig. 2 shows the result in form of a so-called trailed spectrogram. The difference profiles as a function of the radial velocity of Hα in the rest frame of the primary are shown in dependence of the orbital phase. The phase 0.0 is defined as the primary eclipse. To guide the eye the phase axis is extended to the interval from minus 0.5 to 1.5. The intensity of the difference profiles is color-coded. Red means excess emission and blue absorption.
The emission shows a prominent S-shape as a function of the orbital phase with a strong emission red shifted in the phase interval [0.08, 0.29] and blue shifted in the phase interval [0.57, 0.78]. This structure was called single peak emission by Richards et al. [1]. In the following, this notation will be used. The S-shape reflects the orbital movement of the emission source around the primary.

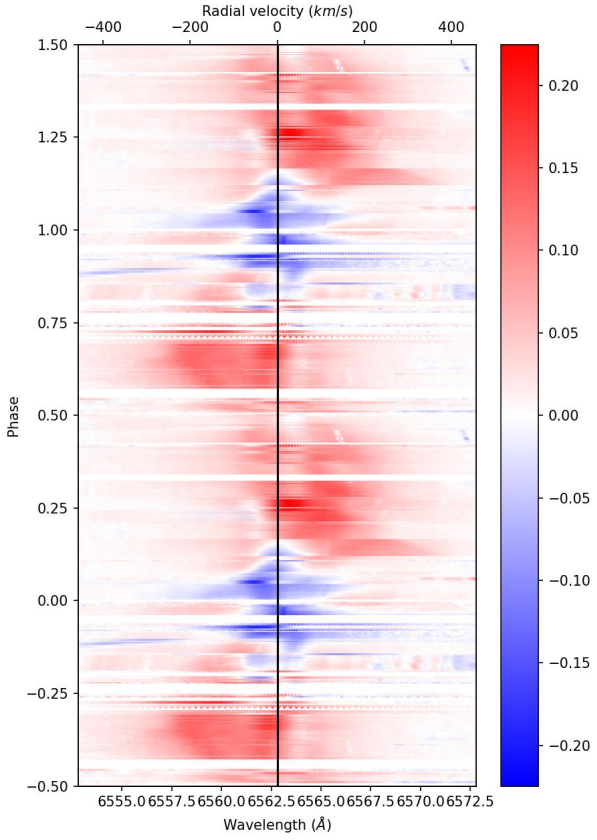

Fig. 2: Trailed spectrogram of the difference profiles of all measured spectra in the observation period 2014 – 2019. The lower x-axis shows the wavelength in the rest frame of the primary and the upper axis the corresponding radial velocity.

Around an orbital phase of 0.5 the emission is weaker and shows two emission peaks. This feature is called double peak emission in [1].

If one analyzes the intensity of the difference profiles at the radial velocity of the primary along the black line in fig. 2, one finds a strong absorption around the primary eclipse at a phase $\Phi = 0.0$. The absorption changes to emission at $\Phi = 0.2$. The red shifted emission achieves a first maximum around $\Phi = 0.3$, a minimum around $\Phi = 0.5$, and a blue shifted second maximum around $\Phi = 0.7$. Finally, it changes to absorption around $\Phi = 0.85$.

As the difference profiles were calculated by a subtraction of the photosphere model from the measured spectra, positive values of the difference profiles show directly the intensity of an emission profile of circumstellar material. On the other hand, negative difference profiles indicate an additional absorption of the material, but the strength of the absorption is not given quantitatively by the intensity of the difference profiles. This follows from the total absorption of two absorbing layers as the product of the absorptions of the single layers instead of their sum.

Rossiter – McLaughlin effect

Figure 3 shows an enlarged part of the trailed spectrogram of fig. 2. The absorption structure around $\Phi = 0.0$ is visible in more detail. The absorption structure appears blue shifted for $\Phi > 0.0$ and redshifted for $\Phi < 0.0$.

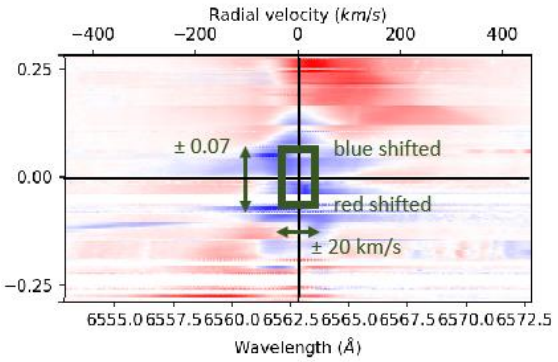

Fig. 3: Enlarged part of the trailed spectrogram from fig.2. The green rectangle indicates the area, in which the rotational effect is expected. The S-shaped absorption structure is visible in the green marked area.

A similar observation of the radial velocity of the photospheric Hα absorption line of β Per was made in 1924 by D.B. McLaughlin [14]. He found a red shifted Hα absorption before the eclipse and a blue shifted one afterwards with an amplitude of ± 20 km/s. This effect was found in an interval of the orbital phase $\Phi = [- 0.07, + 0.07]$. The corresponding area is marked as a green rectangle in fig. 3.

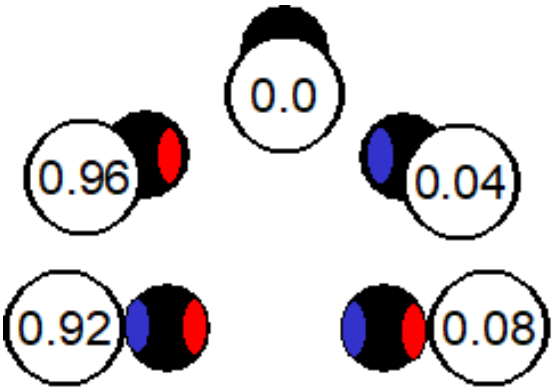

Fig. 4: Rossiter-McLaughlin effect for an eclipse of a rotating star like β Per. The colors mark the red shifted hemisphere of the star (red) and the blue shifted hemisphere (blue). During the partial eclipse, only one hemisphere of the star is visible, resulting in a red shifted spectrum before and a blue shifted spectrum after the primary eclipse. The numbers give the orbital phase.

This so-called Rossiter - McLaughlin effect or rotational effect occurs due to the rotation of the eclipsed star. It was discovered by R.A. Rossiter in 1922 for β Lyr and two years later for β Per by D.B. McLaughlin. The situation of the primary eclipse of β Per is sketched in fig. 4. The rotating primary star has an escaping hemisphere (red) and an approaching hemisphere (blue). At the beginning of the eclipse ($\Phi = 0.96$) only light from the escaping hemisphere is detected. The resulting spectral line shows an overall redshift. At the central eclipse light from both hemispheres contributes equally to the spectral line, hence the rest wavelength of the spectral line is observed. After the eclipse at $\Phi = 0.04$ the spectral line appears blue shifted.

The trailed spectrogram in fig. 3 shows clearly the Rossiter - McLaughlin effect. Some errors remain still present. The red and blue shifted parts are not symmetrically. A more detailed discussion on the accuracy of our data will follow in a next paragraph.

Model of the circumstellar material

Richards et al. presented a model in ref. 1, which describes the origin of the two components found in the trailed spectrogram: the strong single peak and the weak double peak emission. A sketch of this model is shown in fig. 5.

The source of the relatively strong single peak emission is a hot localized region (LR). This region is placed roughly on the connection line between the stars and seems to correlate to the gas stream from the secondary to the primary. Around the orbital phases 0.25 and 0.75 the LR is visible in emission. Around primary eclipse it is placed in the line of sight to the primary and

appears in absorption. Around Φ = 0.5 it is eclipsed by the secondary and therefore not visible for an observer.

A disc-like structure surrounding the primary is the source of the weak double peak emission. Because it is quite weaker than the single peak emission, it is only visible, when the LR is eclipsed around Φ = 0.5.

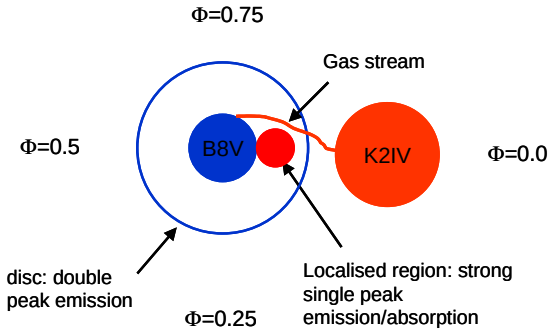

Fig. 5: Model of the circumstellar material in β Per. The primary B8V star is surrounded by a disc like structure, which is the source of the double peak emission. A localised region is the source of the single peak emission. Further, the secondary star and the gas stream are shown.

A more detailed view on the geometry and the resulting visibility of the LR to an observer is given in fig. 6. The arrows show the observer's view directions. The LR appears in emission, in absorption or is invisible due to an eclipse by the primary. The red arrows indicate the directions, where the LR is observable in emission and in absorption at the same time. The corresponding orbital phases from the spectra are also noted. The transition directions give a measure of the geometrical size of the LR.

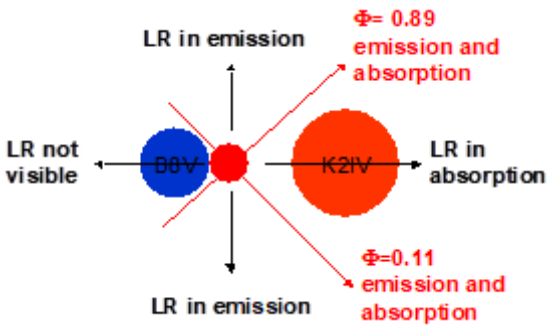

Fig. 6: Geometrical model of the visibility of the localised region (LR) in β Per. The directions of view are indicated by arrows, in which the LR is not visible, in which it appears in emission and in absorption. The red arrows show the directions, in which a transition between emission and absorption is observed.

Accuracy of the difference profiles

The accuracy of the difference profiles is limited by the accuracy of the photosphere model, which was used to calculate the difference profiles, and the quality of the measured spectra itself. The accuracy of the photosphere model is significantly limited mainly because of two reasons:
1. The model used in the analysis is based only on the photosphere of the primary star. The contribution of the secondary and the tertiary stars to the Hα absorption line was neglected. Especially the tertiary star with its spectral type F1V should significantly contribute to the Hα absorption line.
2. During eclipse the photospheric Hα absorption line is influenced by the flux contribution of both eclipsing stars, the limb darkening, the gravitational (deformation) effect, the reflection effect and the rotational (Rossiter – McLaughlin) effect, which all have to be considered in an accurate photosphere model to describe the full eclipse situation.

A major difficulty of the measured spectra are quite different spectral responses of the equipment used. For example, the LHiResIII spectrograph shows a spectral response function, which is not fully understood so far. But there is confidence that our normalization method is able to correct the influence of the spectral response function sufficiently. Hence, we expect sufficient quality of our measured spectra not limiting the resulting data.

In summary, the major limiting factor of the accuracy of our method is assumed being the photosphere model. Therefore, the accuracy of the data obtained by Richards et al. could not be achieved so far.

3. Discussion: Model of the circumstellar material in velocity space

For a more detailed discussion of the circumstellar material the concept of velocity coordinates will be introduced in the following section. Figure 7 shows a model of the β Per binary system in the common position coordinates.

The coordinate system is defined with the primary located in its origin and the secondary fixed on the x axis. The coordinate system rotates with the secondary around the primary. In fig. 7 the direction to an observer at an orbital phase of 0.25 is shown. The blue line shows the outer surface of a Keplerian disc around the primary. the inner surface of the disc is shown as a dashed line.

The same model for the orbital phase 0.25 is shown in fig. 8 in velocity coordinates.

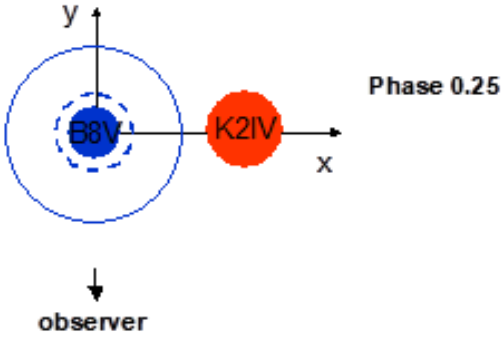

Fig. 7: Model of the β Per binary in position coordinates. The primary and the secondary are shown together with a Keplerian disc around the primary with an inner surface (dashed) and an outer surface (solid line). The system is shown as it appears for phase 0.25 for an observer.

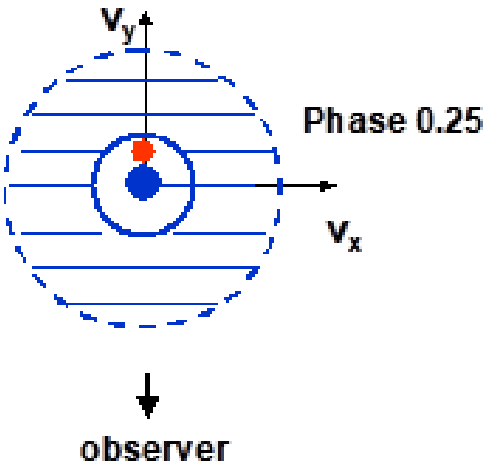

Fig. 8: Model of the β Per binary in velocity coordinates. The primary and the secondary are shown with a Keplerian disc around the primary. The inner surface of the disc in position coordinates appears as the outer surface of the disc in velocity coordinates (dashed). The system is shown as it appears for phase 0.25 for an observer.

The primary is still fixed in the origin of the velocity coordinate system. The v_y coordinate gives the radial velocity measured from the observer. The secondary is located on the v_y axis, because at phase 0.25 the observer measures a maximum positive radial velocity of the star. The accretion disc still forms circles in velocity space coordinates, but the outer surface of the disc in position coordinates (solid line) is located close to the primary in velocity coordinates, because the rotation velocity on the outer surface of the disc is low. The inner surface in position coordinates (dashed line) with a maximum rotational velocity of the disc forms the outer surface in velocity coordinates. Blue straight lines show regions with a specific radial velocity of the disc.

A detailed introduction to velocity coordinates is given in ref. 15.

The advantage of using velocity space coordinates is a very close relation to the measured radial velocity spectral profiles. This is demonstrated in fig. 9. A disc with a hot region is shown in velocity space coordinates. The spectral profiles show the measurement of an observer at the specific orbital phases $\Phi = 0.25$ (profile on the right) and $\Phi = 0.5$ (lower profile). The measured spectral profiles are similar to the projection of the velocity space image of the disc into the direction, which corresponds to a specific orbital phase for an observer. The intensity of the profile is the integral of the velocity space image in the specific projection direction, which is indicated by the length of the thin blue lines in fig. 9. The red arrows mark the position of the emission from the hot region in the measured spectral profiles.

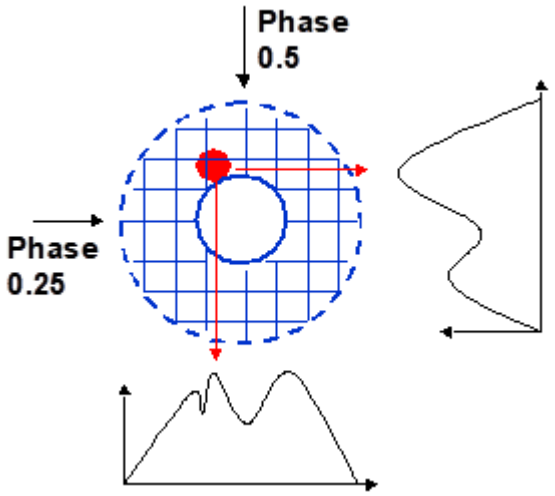

Fig. 9: A disc (blue) with hot region (red) in velocity space coordinates and the measured emission spectra for two different orbital phases. The measured spectra are the projection of the velocity space image into a direction that corresponds to a specific orbital phase for an observer. In this diagram, the observer moves around the disc as a function of orbital phase.

Due to the orbital rotation of the hot region around the star the measured radial velocity of the emission peak v_r moves through the spectral profiles as a function of the orbital phase Φ. The radial velocity follows the equation

$$v_r(\Phi) = v_y * \sin(2\pi\phi) - v_x * \cos(2\pi\phi) + Y \qquad (1)$$

where v_y and v_x are the velocity space coordinates of the hot region. The constant Y does not vanish for inclination different from 90° and if a movement in z-direction occurs.

Fig. 10 shows a graph of equation (1) as an example. Here Y was set to zero and the phase as

well as the amplitude of the maximum depend on the velocity space coordinates v_y and v_x.

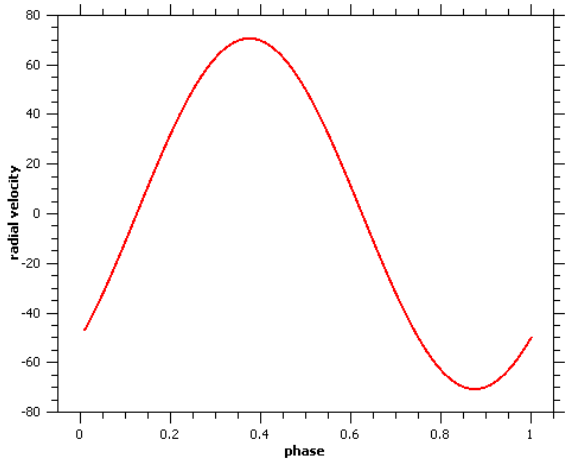

Fig. 10: The radial velocity of a hot region rotating around a star as a function of the orbital phase follows a graph according to equation (1), v_x = 50 km/s, v_y = 50 km/s.

In the following, a quantitative analysis is described to investigate the structures in the difference profiles in velocity space coordinates. The intensity and the radial velocity of the two strongest maxima in each of the difference profiles were then determined. It was assumed that the maxima with a positive radial velocity in the phase interval [0.10, 0.45] and a negative radial velocity in the phase interval [0.55, 0.90] correspond to the single peak emission.

In fig. 11 the intensity of these maxima is shown as a function of the orbital phase.

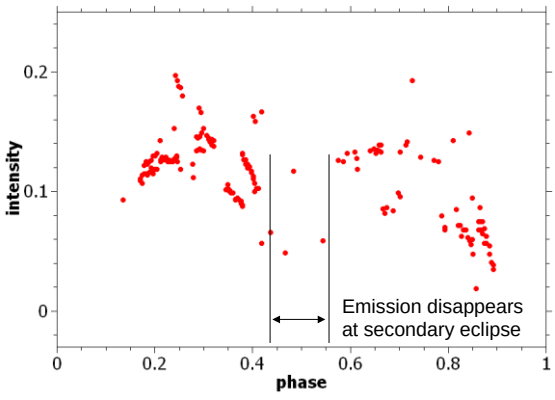

Fig. 11: The intensity of the maxima in the difference profiles as a function of the orbital phase. Only maxima of the single peak emission were considered. The single peak emission shows a minimum around Φ = 0.5, which indicates the eclipse of the localised region by the primary.

The single peak emission shows high intensities around an orbital phase of Φ = 0.25 and Φ = 0.75. It shows a minimum intensity between Φ = 0.45 and Φ = 0.55 indicating that the LR as the source of the single peak emission is eclipsed by the primary.

In fig. 12 the radial velocity of these maxima is shown as a function of the orbital phase. The measured radial velocity of the single peak maxima (red symbols) was fitted by using (1). A fit for Y = 0 is shown as a black line and a fit with a non-vanishing Y is shown as a blue line.

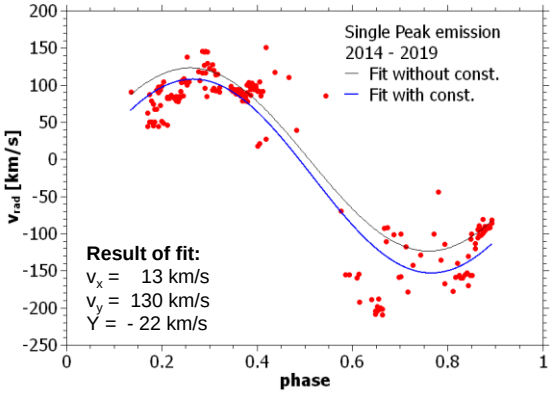

Fig. 12: The radial velocity of the maxima in the difference profiles as a function of the orbital phase. Only maxima of the single peak emission were considered. In addition to the measured data the result of two fits by using equation (1) are shown.

The blue line fit with a non-vanishing constant Y matches better to the data than the black line fit.

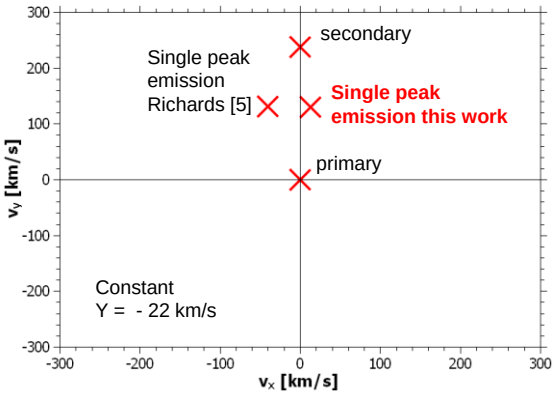

Fig. 13: Doppler map of the β Per binary. The primary is located in the coordinate origin. The position of the single peak emission source from our data is shown in comparison to the corresponding position from ref. 5. Further, the position of the secondary is shown.

It is shown in ref. 7 by means of 3D tomography that a flow in z-direction exists, which is probably driven by the magnetic field of the secondary. Hence, we assume that our result containing a non-vanishing constant Y fits reality better.

In a next step the velocity space coordinates determined from the fit were put in an adequate velocity space coordinate system. The resulting graph is called Doppler map and is shown in fig. 13.

A Doppler map is a velocity space diagram. To transform a Doppler map into position coordinates additional assumptions of the system, e. g. a Keplerian velocity field, are needed. In fig. 13 the coordinate axes were chosen in such a way, that v_y corresponds to the measured radial velocity for the orbital phase 0.25 of the binary.

The primary is placed in the coordinate center and the secondary on the v_y axis in fig. 13. The LR, which is the source of the single peak emission, is located at
v_x = (13 ± 5) km/s and
v_y = (130 ± 5) km/s.
The error of the velocity coordinates is the accuracy of the fit.

The orbital velocity v_y of the LR is about the half of v_y of the secondary. It obeys a relatively low velocity in *x*-direction, which means it is located closely on the connection line between the stars. The positive value of v_x indicates that the LR slightly follows the orbital rotation of the secondary.

The velocity coordinates of the LR from ref. 5 based on spectra taken 1976/77 are shown in fig. 13 for comparison. The v_y position is similar to the presented data, whereas ref. 5 reports a slightly negative v_x position meaning a preceding of the LR with respect to the secondary. With the currently limited accuracy of the difference profiles described above, it cannot be decided whether this difference is real.

The radial velocity of the maxima of the single peak as well as of the double peak emission are shown in fig. 14. Each observing period is separated by different colors allowing for a search of temporal variabilities.

The data from different observation periods do not obviously show any differences regarding a temporal variability of the emission regions between 2014 and 2019. A possible detection of a variability is difficult, because the number of spectra is quite inhomogenously distributed over the observation time interval.

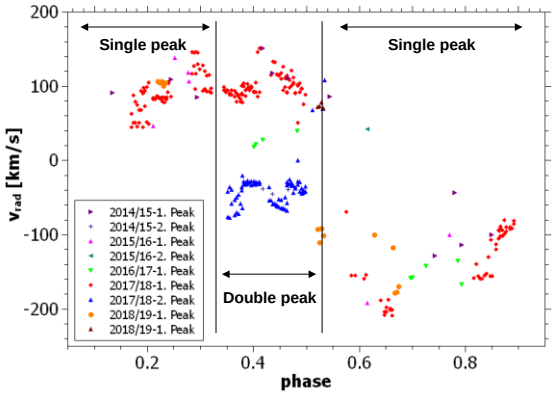

Fig. 14: The maxima of the difference profiles of the single peak and the double peak emission are shown color coded for the specific observation periods. “1. Peak” means single peak emission and “2. Peak” double peak emission in the legend. No temporal variability is visible.

4. Summary and Outlook

We measured Hα spectra of β Per between 2014 and 2019 at three amateur observatories equipped with different spectrographs. The spectra were evaluated in a similar way as described by Richards et al. [1, 5]. This allowed a comparison of the accuracy of the presented data as well as a search for significant temporal variabilities in the circumstellar material in the β Per system between the mid 1970s and today.

The accuracy of the presented data is limited mainly due to the use of a simplified photospheric model to calculate the difference profiles from the measured spectra. So far, only the photosphere of the primary was considered in the model. Contributions of the secondary and the tertiary star to the Hα absorption line as well as eclipsing effects to the spectral flux were neglected. For the future we plan to improve our model to achieve a comparable data quality to that of Richards et al.

By comparing the velocity coordinates in a Doppler map with the coordinates determined by Richards et al. a reasonable agreement was found. The judgment over the observed small shift in v_x cannot be done yet due to the limited accuracy of our data.

In ref. 5 an image reconstruction by applying the so-called Doppler tomography method is presented. After improving the accuracy of our difference profile extraction method, the application of the Doppler tomography is planned to achieve a direct comparison of images of the circumstellar material from the mid 1970s and from today.

Acknowledgments

We thank to Enrico Gerlach and Thomas Hunger for a lot of fruitful discussions.

References

[1] M.T. Richards et al, Astrophys. J. Sup. Ser. 86 (1993) 255
[2] 9th Catalogue of spectroscopic binary orbits, http://sb9.astro.ulb.ac.be
[3] R.T. Zavala et al., Astrophys, J. Lett. 715 (2010) 44 and 843 (2017)18
[4] B. Bitnar, Spektrum 52 (2017) 4
[5] M.T. Richards et al, Astrophys. J. 459 (1996) 249
[6] M.T. Richards, Astron. Nachr. 325 (2004), 229
[7] M.T. Richards et al. Astrophys. J. 760 (2012) 8
[8] M.T. Richards et al, Astrophys. J. Sup. 88 (1993) 199
[9] U. Waldschläger, Spektrum 53 (2018), 17
[10] U. Zurmühl, Spektrum this issue (2019)
[11] P. Schlatter, http://www.peterschlatter.ch/SpectroTools
[12] vizier.u-strasbg.fr/viz-bin/VizieR-2, POLLUX database, input parameters: T= 12500K, g= 4
[13] C. Brock, Spektrum this issue (2019)
[14] D.B. McLaughlin, Astrophys. J. 60 (1924) 22
[15] T.R. Marsh, K. Horne, MNRAS. 235 (1988). 269

Bernd Bitnar is a physicist. Professionally, he deals with the development of power electronics chips. As an amateur astronomer, he looks back on many years of deep sky photography. Stellar spectroscopy has been a new challenge for some years and is being pursued in his small roof-top observatory.

During daytime **Christian Brock** programs algorithms to optimize cellular networks. At night he attends to visitors at the Dresden-Gönnsdorf Observatory, supervises students, does some visual observations by himself and cooperates in the Dresden spectroscopy group.

Uwe Zurmühl had a strong interest in astronomy since his days of youth, observing sunspots and planets with a 40 mm refractor at the age of 12. He studied physics at the University of Göttingen, where he received his Ph.D. in 1983. After some years of research in medium energy physics, he has worked in the industry in the field of software engineering. Since 2015 his astronomical activities are focused on spectroscopy, mainly on investigating the application of transmission gratings.

Ulrich Waldschläger is a physicist and has been working in the field of industrial research on the development of energy-dispersive X-ray analysis devices for 24 years. Since 2012, he has been working on astronomical spectroscopy on the outskirts of Berlin in his free time.

ASpekt 19 – Jahrestagung in Salzburg, 3.-5. Mai 2019

U. Thomas Hunger* und Herbert Pühringer+
* Weinbergstraße 12, 01129 Dresden, Germany, E-Mail: thunger03@web.de (Corresponding author)
+ Wiesenweg 4A, 5102 Anthering, Austria, E-Mail: pherby@gmx.de

Zusammenfassung
Es wird von der Jahrestagung der Fachgruppe Spektroskopie an der Vega-Sternwarte, Salzburg, Österreich, berichtet. Die einzelnen Vorträge werden in chronologischer Reihenfolge rekapituliert. Die Teilnehmer werden eine interessante und gelungene Konferenz in Erinnerung behalten.

Abstract
It is reported on the annual meeting of the section Spectroscopy at the Vega Observatory, Salzburg, Austria. The individual talks are recapitulated in chronological order. The participants will remember an interesting and successful conference.

Received: 2019-10-17, Revised: 2019-11-04, Accepted: 2019-11-12

Die Jahrestagung der Fachgruppe führte in diesem Jahr in die Nähe von Salzburg nach Österreich, wo wir Gäste der VEGA-Sternwarte des Hauses der Natur am Haunsberg in Obertrum sein durften.

Dieses Jahr mussten Im Vorfeld einige organisatorische und krankheitsbedingte Hürden genommen werden. So wurde die Erstellung des finalen Programms z.B. sehr kurzfristig durch Thomas Eversberg geleistet.

Zum Gelingen der Veranstaltung vor Ort, hatte dann aber insbesondere die Betreuung durch Herbert Pühringer und dem Team der Arbeitsgemeinschaft Astronomie beigetragen.

Dazu gehörte z.B. auch, dass für Interessierte im Vorfeld der Konferenz ein Beobachtungs-Meeting ermöglicht wurde. Befördert durch die günstige Feiertagssituation in Deutschland nutzten eine Reihe von Teilnehmern die Gelegenheit sich mit den vorzüglichen Beobachtungsbedingungen vor Ort vertraut zu machen. Herbert ermöglichte ganz ungewohnte Blicke durch das 1m-Teleskop auf bekannte Deep-Sky-Objekte. Außerdem konnte noch am lebenden Objekt, einem fasergekoppelten Spektrographen, erfolgreich justiert werden. Es soll nicht unerwähnt bleiben, dass gerade zu diesem Zeitpunkt die temporären Wetterbedingungen einem Lotto-Gewinn gleichkamen. Regen und Schnee in den folgenden Tagen sollten das dann noch deutlich machen.

Die eigentliche Tagung startete am Freitagabend mit einem gemeinsamen Abendessen im Hotel Ammerhauser, Anthering am Fuße des Haunsberges. Herbert nutze die Gelegenheit, die Teilnehmer herzlich zu begrüßen und organisatorische Fragen wie die Festlegung der Sitzungsleiter und -innen zu klären.

Abb. 1: Die idyllisch gelegene Vega-Sternwarte.

Die Tagung auf der Sternwarte wurde am Samstag durch Herbert eröffnet. Er erwähnte, dass die ASpekt 19 die erste wissenschaftliche Tagung an der Vega-Sternwarte ist – im Jahresverlauf sollten noch zwei weitere folgen. Der Leiter des Hauses der Natur, Herr Dr. Winding, gab uns seine Referenz. Die Einleitung endet

mit einem beeindruckenden Video zur Sternwarte und den Aktivitäten der Arbeitsgemeinschaft.

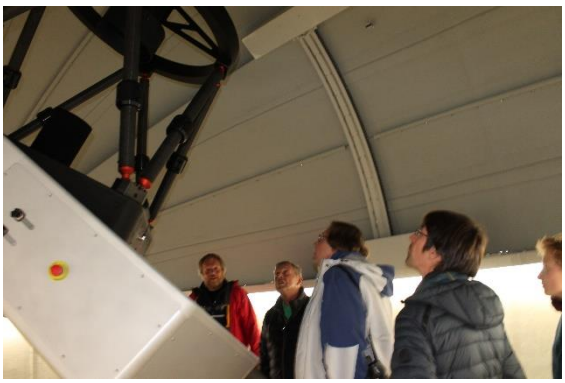

Abb. 2: Begeisterung am 1m-Teleskop.

Der vormittägliche Vortragsblock wurde durch Thomas Hunger geleitet und startete mit einem Beitrag von Thomas Eversberg zur Fachgruppe und sollte – auch unterstützt durch ein Thesenpapier – Anregung für die sonntäglichen Diskussionen sein. Dazu mehr unten im Text.

Bernd Bitnar startete dann seine Ausführungen zum aktuellen Stand der „Studie über zirkumstellares Material bei β Persei“. Das Gemeinschaftsprojekt mit Christian Brock, Ulrich Waldschläger und Uwe Zurmühl beobachtet seit mehreren Jahren die physikalischen Vorgänge an der Akkretionsscheibe dieses Archetyps der Bedeckungsveränderlichen.

Nach einer kurzen Kaffeepause berichtete Huib Henrichs, zur „Simultanen Photometrie und Spektroskopie des außergewöhnlichen Asteroiden 3200 Phaethon mit einem Shelyak Alpy-Spektrographen an einem C9.25-Teleskop“. Huib ist emeritierter Astronomie-Professor der Freien Universität Amsterdam und stieß erstmals zur Fachgruppe. Er stellte im Vortrag seine automatisierte private Flachdach-Sternwarte und seine Beobachtungsinteressen, vor allem die massiven O- und B-Sterne, vor. Am Beispiel von Phaeton zeigte er die erfolgreiche Klassifizierung „C-Komplex Typ B“ von Asteroiden.

Den abschließenden Vortrag am Vormittag hielt Tony Moffat – vielen ein Begriff von den bisherigen Teneriffa-Kampagnen. Sein Vortrag behandelte neue Ergebnisse an massiven Sternen auf Basis der Beobachtungen mit den BRITE Satelliten und zusätzlichen erdgebundenen spektroskopischen Untersuchungen, zu denen auch Amateure beigetragen haben. Das gemeinsame Mittagsessen wurde im Anschluss im Gasthaus "Zur Kaiserbuche" ganz in der Nähe der Sternwarte eingenommen.

Abb. 3: Blick ins Plenum

So gestärkt ging es mit nachmittäglichem Elan im Programm weiter, durch das Gerrit Grutzeck führte. Erste Redner war Ulrich Waldschläger zu seinem „Selbstbau-Echelle-Messplatz „E1“ für spektrale Auflösungen bis R=30.000“. Der Bericht umfasste die verschiedenen Prototypenstufen, die vielen Lernschritte, die Selbstbau-Kalibrationslichtquelle und schließlich thermische Stabilitätsoptimierungen.

Anschließend referierten zunächst Robert Kallinger, Matteo Kucher und Nikolaus Webersberger (Spektroskopiepreisträger 2018) über den Status ihres Selbstbauspektrografen, wie in Sankt Niklasen und Frankfurt versprochen. Über die Funktionsweise konnten wir uns während der Pausen und in der eingangs erwähnten Beobachtungsnacht direkt informieren. Ein tolles Gerät mit vielen gekonnt ausgeführten Detaillösungen!

Paolo Sereni und Herbert Pühringer berichteten zum nunmehr an der VEGA verfügbaren Echelle-Spektrographen FLECHAS der CAOS Gruppe. Paolo erläuterte seine Vorstellungen zur Zusammenarbeit mit der Universität Salzburg.

Abschließend trugen noch die CAOS-Granden Gerardo Ávila, Carlos Guirao und Jésus Rodrigúes zu „Removing the blaze effect of an Echelle spectrum with MIDAS“ vor. Die BACHES Routinen sind jetzt in der MIDAS Distribution enthalten.

Nach einer ausführlichen Kaffeepause, die gut wie alle anderen zeitlich reichlich bemessen Pausen für Diskussionen genutzt wurde, berichtete Christoph Quandt zum „Projekt Gelbe Überriesen“. Er fasste den aktuellen Stand der ρ Cas Kampagne zusammen, zu der immer mehr Beobachter beitragen.

Erstmals fand – angeregt und moderiert durch Thomas Eversberg – ein Runder Tisch zum Thema „Techniken der Datenanalyse“ statt. Teilnehmer auf der Bühne waren Bernd Bitnar,

Huib Henrichs, Tony Moffat und Christoph Quandt. Tony hatte eine umfangreiche Dokumentation vorbereitet, die als roter Faden zu den Themen Trennung spektroskopischer Doppelsterne, Graustufenplots, Periodensuche, Linienmomente, Anpassung der Radialgeschwindigkeiten, Kreuzkorrelation und Kollidierende Winde diente. Zusammen mit dem Auditorium ergaben sich lebhafte Diskussionen, so dass die Zeit am Ende nicht reichte, alle geplanten Aspekte anzusprechen. Zeit zur Fortsetzung von intensiven Diskussionen war aber beim gemeinsamen Abendessen im Ammerhauser mit anschließendem, gemütlichem Beisammensein gegeben.

Abb. 4: Blick zur Bühne während des Runden Tisches.

Erwähnt sollen noch die Posterbeiträge werden. Huib hatte begleitend zu seinem Vortrag ein Poster bereitet, Uwe Zurmühl präsentierte „Transmission Gratings in Convergent Beam“ und „Variable Stars on the Asymptotic Giant Branch“.

Der Sonntag begann mit einem (angekündigten) Schneeschock. Der Wetterbericht hatte Schneefall auf dem Haunsberg vorhergesagt, wobei nicht ganz klar war, wieviel von der weißen Pracht eintreffen würde. Herbert hatte aber zusammen mit dem Bürgermeister für alle Fälle vorgesorgt. So konnte das Vortragsprogramm planmäßig unter der Sitzungsleitung von Josefine Liebisch beginnen.

Thomas Eversberg ging in seinem Vortrag der Frage nach: „Flat-Fields–Wofür sind die eigentlich?“ Thomas wies auf die grundliegende Bedeutung der Flats als Basis für eine Kontinuumsanpassung niedriger Ordnung und der Vermeidung scheinbarer Oszillationen hin. Thematisiert wurden weiterhin Strategien zum richtigen Signal-zu-Rausch-Verhältnis der Flats („Mache 10-20 Flataufnahmen“) und der Datenreduktion von Spektren.

Anschließend referierte Gerrit Grutzeck zu einem für optische Spektroskopiker eher ungewöhnlichen Spektralbereich: Radiowellen. Nach einer grundlegenden Einführung in die (instrumentelle) Radioastronomie erfolgte eine Beobachtung an SALSA zur Messung der Geschwindigkeits-verteilung des kalten Wasserstoffs in der Milchstraße. Das war Radiospektroskopie live und durchaus eine thematische Bereicherung der Tagung.

Nach der Kaffeepause ging es mit einem Vortag von Jan Sundermann zu Polarisationseffekten in der Spektroskopie weiter. Bei der Wiederinbetriebnahme eines Merzrefraktors mit Sonnenprisma gab es interessante Effekte beim spektroskopischen Einsatz. Thomas Eversberg moderierte den anschließenden zweiten Teil der Fachgruppenthemen. Nach dem Rücktritt des Fachgruppensprechers konnte kein(e) Kandidat(in) für die Aufgabe gewonnen werden. Daher werden die Stellvertreter die Arbeit zunächst kommissarisch fortsetzen. Diskutiert wurde ferner das Statut, es bleibt zunächst in seiner Form erhalten. Die Beteiligung am Forum ist durch abnehmende Aktivität gekennzeichnet. Klare Gründe wurden nicht ermittelt, aber festgestellt, dass Anfänger besser abgeholt und motiviert werden sollen. Für das FG-Journal wurde kein akuter Änderungsbedarf festgestellt bis auf die Fakten Artikelanzahl und Erscheinungstreue. Der teils mangelnde Präsenz im VdS-Journal für Astronomie wurde angemerkt, ohne aber dahingehende Beschlüsse zu fassen.

Zum Abschluss der ASpekt gaben Christoph Quandt und Knud Henke einen Vorausblick auf das kommende Jahr in Lübeck. Die Jahrestagung wurde von Herbert mit Hinweis auf großzügigen freien Eintritt am Sonntag ins Haus der Natur abgeschlossen. Nach einem Mittagessen in der Kaiserbuche erfolgte die Heimfahrt der Teilnehmer. Es bleiben wieder einmal sehr schöne Erinnerungen an eine letztendlich erfolgreiche Konferenz in einem wunderbar geeigneten Ambiente. Herzlichen Dank an das Team vor Ort dafür

Abb. 5: Gruppenbild.

Thomas Hunger beschäftigt sich seit seiner Schulzeit mit Astronomie. Das Interesse an der Astrospektroskopie wurde im Physikstudium geweckt. Seitdem wird mit Objektivprisma, Staranalyzer und neuerdings einem LHiRes III in Drebach und Gönnsdorf beobachtet, soweit es die Freizeit zulässt. Höhepunkte waren die Teilnahmen an den zwei Teneriffa-Beobachtungskampagnen der Fachgruppe, in der er seit 1998 Mitglied ist. Von 2000 bis 2013 war er VdSJ-Fachredakteur und FG-Sprecher im Zeitraum 2009-2013, aktuell Sprechervertreter und seit 2009 Chefredakteur des Spektrums.

Herbert Pühringer ist Mitglied der Arbeitsgruppe Astronomie am Haus der Natur in Salzburg. Er leitet seit 15 Jahren den Pluskurs Astronomie für interessierte Schüler im Land Salzburg.

Your Fachgruppe still needs you!

Administrator (m/w/d) für die Fachgruppenwebseite gesucht!

Seit über einem Jahr ist Webmasterposten verwaist! Dies ist an der Aktualität der Webseite für alle sichtbar. Bitte überdenke, ob Du nicht für die Fachgruppe aktiv tätig werden willst.

Bei Interesse bitte bei Thomas Eversberg oder Gerrit Grutzeck melden.

ASpekt20

Jahreskonferenz der Fachgruppe Spektroskopie in der VdS e.V.

Annual Conference of Section Spectroscopy of German Amateurastronomical Society VdS e.V.

12.-14. Juni 2020, Johanneum Gymnasium, Lübeck

Anmeldeschluss/Registration Deadline: 01.04.2020

Zu dieser Tagung laden wir alle spektroskopisch interessierten Astronomen ein, insbesondere EinsteigerInnen und junge Kolleginnen und Kollegen. Eine VdS-Mitgliedschaft ist nicht nötig. Mit Vorträgen und einer Poster- und Gerätesession aus dem Teilnehmerkreis (Vortragsanmeldungen beim Tagungsteam) tauschen wir uns aus und besprechen offene Fragen zur Spektroskopie.

Detaillierte Informationen / Detailed information:
http://spektroskopie.vdsastro.de/konferenz.html

Anmeldung / Registration: aspekt@sternwarte-luebeck.de

unter Angabe folgender Informationen:
Name und vollständige Postadresse mit PLZ, Ort, Straße, Hausnummer, Land, E-Mail-Adresse
Tag und Tageszeit der voraussichtlichen An- und Abreise, Personen- und Zimmerzahl bei Hotelbuchung

Tagungshotel ist das Motel One, der reduzierte Tagungspreis beträgt 79€ pro Zimmer und Nacht.
Die Hotelbuchung erfolgt über die Sternwarte Lübeck. Die Kontoverbindung ist
Kontoinhaber: Arbeitskreis Sternfreunde Lübeck e.V.
Bank: Sparkasse zu Lübeck, IBAN: DE64 2305 0101 0002 2095 00, BIC: NOLADE21SPL

Für junge Teilnehmer haben wir einen Hilfsfond eingerichtet, mit dem wir auf Anfrage einen vertraulichen Zuschuss anbieten können.

Workshop "Grundlagen der Sternspektroskopie mit dem Baader DADOS-Spaltspektrografen"

Dozent: Dipl.-Phys. Bernd Koch, Bernd.Koch@astrofoto.de
Termin: 20. - 23. März 2020
Kurszeit: Freitag 18 Uhr bis Sonntag ca. 15 Uhr
Ort: Carl-Fuhlrott-Gymnasium, Jung-Stilling-Weg 45, Wuppertal
Kursgebühr: 140€ p.P.
Hinweise zu Übernachtungsmöglichkeiten nahe der Sternwarte können gegeben werden.

https://www.baader-planetarium.com/de/blog/grundlagen-der-sternspektroskopie-mit-dem-baader-dados-spaltspektrografen/

Workshop „Objektbezogene Astrospektroskopie für Amateure“

Dozent: Ernst Pollmann, ernst-pollmann@t-online.de
Termin: 01. - 03. Mai 2020
Kurszeit: Freitag 18 Uhr bis Sonntag ca. 15 Uhr
Ort: Carl-Fuhlrott-Gymnasium, Jung-Stilling-Weg 45, Wuppertal
Kursgebühr: 110€ p.P.
Anmeldeschluss 26. April 2020, 12Uhr.

https://www.baader-planetarium.com/de/blog/objektbezogene-astrospektroskopie-fuer-amateure/

Nur für Mitglieder der Fachgruppe Spektroskopie in der
Vereinigung der Sternfreunde e.V.

For members of the Section Spectroscopy
of the Society of German Amateur Astronomers only.

Besuchen Sie / Visit

http://spektroskopie.vdsastro.de

und werden Sie Mitglied. Einfach per Mail an den Sprecher der Fachgruppe.

and become a member by sending an e-mail to the spokesman of the section.